Available online at www.sciencedirect.com
SCIENCE DIRECT®
ELSEVIER
Geomorphology 60 (2004) 37–72
GEOMORPHOLOGY
www.elsevier.com/locate/geomorph

An incision wave in the geologic record, Alpujarran Corridor, southern Spain (Almería)

A.F. García[a,b,*], Z. Zhu[c,d], T.L. Ku[d], O.A. Chadwick[e], J. Chacón Montero[b,f]

[a] Department of Physics, California Polytechnic State University, San Luis Obispo, CA 93407, USA
[b] Grupo de Investigaciones medio ambientales: riesgos naturales e ingenieria del terreno, University of Granada, Granada, Spain
[c] Guangzhou Institute of Geochemistry, Chinese Academy of Sciences, People's Republic of China
[d] Department of Earth Sciences, The University of Southern California, Los Angeles, CA 90089-0740, USA
[e] Department of Geography and Department of Geological Sciences, The University of California, Santa Barbara, CA 93106, USA
[f] Departamento de Ingeniería Civil, Universidad de Granada, C/ Severo Ochoa s/n 18071, Granada, Spain

Received 13 January 2003; received in revised form 5 July 2003; accepted 19 July 2003

Abstract

The term "incision wave" was coined in the 1990s to describe wave-like patterns of stream incision propagating through numerically modeled bedrock-channel river systems. An incision wave consists of a crest where available stream power is greatest, and where vertical incision is most rapid. The crest is flanked by limbs where there is less available stream power and where vertical incision rates are slower. Farther away from the crest, available stream power is less and incision rates are slower than in the limbs. Modeling results suggest tectonically induced base-level fall triggers incision waves that propagate upstream through bedrock-stream networks. However, it has recently been postulated that the equation underpinning incision-wave models cannot realistically simulate river systems. This paper provides field-geological evidence supporting the hypothesis that tectonically induced base-level fall triggers incision waves that propagate through bedrock-stream networks for tens of kilometers.

Mid and late Pleistocene alluvial morphostratigraphy in the Río Andarax drainage basin, southeast Spain is interpreted to indicate that patterns of paleo stream power were controlled by an incision wave. In the conceptual model proposed in this paper, the signature of an incision wave in the Río Andarax drainage network is recorded by the contrasting morphostratigraphy of oxygen isotope stage 8 ("OIS8") time landforms. At the crest of the incision wave during OIS8, there is no record of a paleoalluvial level because available stream power exceeded critical stream power and streams were incising vertically. The crestal area is flanked by OIS8-time strath terraces, which record the position of the two limbs of the incision wave. Farther upstream, OIS8-time alluvial fills mark an area unaffected by the incision wave.

During oxygen isotope Stage 2 ("OIS2") and/or oxygen isotope Stage 1 ("OIS1"), sediment availability in the Río Andarax catchment was low, and the pattern of relative stream power was threshold-like rather than wave-like. Differences in the manifestation of the incision wave during OIS8 vs. during OIS2 and/or OIS1 indicate that climate and sediment availability can control how incision waves propagate through fluvial systems.

Keywords: Betic Cordillera; Strath terrace; Incision; Drainage evolution

* Corresponding author. Department of Physics, California Polytechnic State University, San Luis Obispo, CA 93407, USA.
E-mail address: afgarcia@calpoly.edu (A.F. García).

0169-555X/$ - see front matter © 2003 Elsevier B.V. All rights reserved.
doi:10.1016/j.geomorph.2003.07.012

1. Introduction

1.1. Incision waves

Bedrock stream research in the 1990s was led by quantitative geomorphologists who used new isotopic dating methods, as well as equations and powerful computers, to model landscape and bedrock-stream network evolution. In particular, numeric simulations and morphometric analyses of landscapes were used to study how base-level fall affects bedrock stream networks (e.g., Seidl and Dietrich, 1992; Seidl et al., 1994, 1997; Safran, 1998; Sklar and Dietrich, 1998). One significant result of these studies is evidence that transient episodes of base-level lowering cause "incision waves" to move upstream through fluvial systems (Fig. 1; Anderson, 1994; Rosenbloom and Anderson, 1994; Safran, 1998).

The most comprehensive evaluation of incision wave-controlled stream entrenchment caused by transient, tectonically induced base-level lowering was conducted by Safran (1998). Computer modeling was used to simulate the 10 Ma to present history of a 32,000-km^2 mountainous drainage basin (Safran, 1998). Bedrock-stream incision was governed by the "stream-power law" (see below), and incision rates for the model were calibrated with fission-track dating of drainage-basin bedrock (Safran, 1998). Numeric simulations of transient episodes of tectonism generated incision waves that moved upstream through the modeled fluvial system (Fig. 1; Safran, 1998). The following is a summary of incision-wave related processes as outlined in Safran (1998), and is herein referred to as "the incision wave hypothesis".

An incision wave consists of a locus of most rapid incision (the wave crest), flanked by two areas of less rapid incision (upstream and downstream limbs). Streams at the crest incise most rapidly because they have been affected by base-level fall for just enough time to steepen their channels significantly, which causes an increase in available stream power. Streams in the downstream limb incise more slowly because they have been affected by base-level fall for more time than streams in the crest and are closer to grade at the new, lower base level. Their channels are less steep, and they have less available stream power than streams in the crestal area. Streams in the upstream limb incise more slowly than in the crest because they have only recently been affected by base-level fall. Their channels have not been steepened as much as channels in the crestal area and, consequently, they have less available stream power.

The fundamental objective of this paper is to show how bedrock-stream incision patterns predicted by the incision wave hypothesis are recorded in a alluvial-

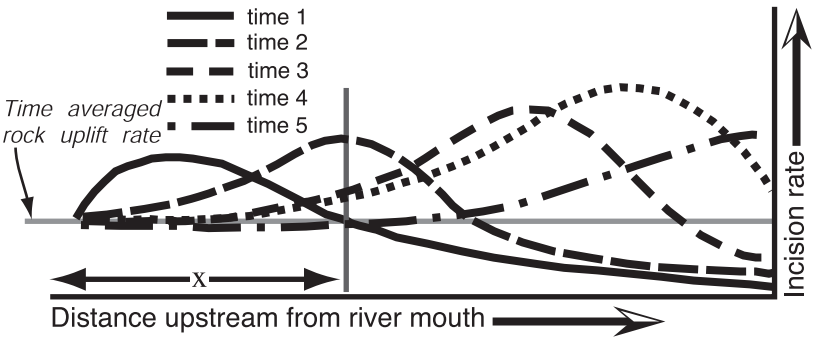

Fig. 1. Schematic representation of how an incision wave moves upstream through a fluvial network in response to transient tectonic uplift. This figure is modified and interpreted from Safran (1998). For the reach of a stream at distance x from the headwaters, incision rate was approximately equal to the rate of rock uplift prior to the pulse of transient tectonic uplift. During time 1 at distance x, incision rates are slower than farther downstream because streams in the lower reaches have been steepened by the recent pulse of base-level fall. Incision rate is greatest at distance x during time 2 because base-level fall has affected the reach at x long enough for it to significantly increase its gradient (this is the crest of the incision wave). By time 3, the channel at x has lowered its bed and is closer to the new local base level. Consequently, its channel is less steep and incision slows (this is the "downstream limb" of the incision wave). Figure used with permission from the author.

stratigraphic sequence. This objective is reached by analyzing and interpreting alluvial morphostratigraphy.

1.2. The incision wave hypothesis and the stream-power law

Since the landmark paper of Howard and Kerby (1983), many landscape-modeling studies used the "stream power law" to simulate bedrock-channel incision (e.g., Seidl and Dietrich, 1992; Seidl et al., 1994, 1997; Safran, 1998; Sklar and Dietrich, 1998). The steam power law relates bedrock channel lowering rate to the product of an empirically derived erosion-efficiency constant (k), drainage area raised to an empirically derived power (m), and channel slope raised to an empirically derived power (n). Modeling studies that generated incision-waves and/or upstream-migrating knickpoints (Rosenbloom and Anderson, 1994; Seidl et al., 1994; Tucker and Slingerland, 1994; Safran, 1998) used a stream power law with single values for k, m, and n to simulate bedrock-stream incision throughout entire drainage basins. Subsequent studies questioned using a stream power law with one value each for k, m, and n, to simulate bedrock incision throughout an entire drainage basin (Sklar and Dietrich, 1998; Stock and Montgomery, 1999; Wohl and Merritt, 2001; Roe et al., 2002). These studies argue that values of k, m, and n can significantly change as a function of time (Sklar and Dietrich, 1998; Roe et al., 2002), and from one reach to the next along a single stream (Sklar and Dietrich, 1998; Stock and Montgomery, 1999; Wohl and Merritt, 2001; Roe et al., 2002). Other bedrock-stream studies showed that in some cases, long-term incision patterns do not fit patterns predicted by the stream power law (Pazzaglia et al., 1998; Pazzaglia and Brandon, 2001).

Questioning the equation that is the basis of modeling studies that gave rise to the incision wave hypothesis also requires questioning whether or not the incision wave hypothesis can account for stream-incision patterns in large drainage basins consisting of reaches having distinctly different morphologies (sensu Wohl and Merritt, 2001; e.g., Anderson, 1994; Safran, 1998). In other words, does the incision wave hypothesis account for incision patterns in large (>a few hundred square kilometers catchment areas) drainage basins, which are inherently heterogeneous? A logical step toward answering this question is to find the signature of an incision wave in the geologic record. Numerous studies have documented migrating knickpoints using stream channel and landscape morphology along reaches of streams that are a few kilometers to 10 km long (e.g., Seidl and Dietrich, 1992; Rosenbloom and Anderson, 1994; Seidl et al., 1994), and up to a few hundred kilometers long (Weissel and Seidl, 1998). The quantitative components of these studies were groundbreaking and contributed greatly to understanding how base-level fall propagates through a fluvial system, but they are based on field evidence that is morphological rather than geological.

Several geological studies have provided examples of upstream-propagating base-level fall. Fluvial morphostratigraphy and morphometric analyses indicate that base level fall triggered by tectonically controlled stream-capture propagated 20 km through the Aguas/Feos river system of southern Spain (Harvey and Wells, 1987; Harvey et al., 1995; Mather and Harvey, 1995; Mather et al., 2002; Stokes et al., 2002). Large-river-system scale knickzone propagation has been documented using fluvial stratigraphy and longitudinal profile analyses (Zaprowski et al., 2001). However, to date, there is no geologic evidence indicating that base-level fall propagates upstream in a wave-like fashion, with a crestal area where available stream power is greatest, flanked by two limbs where available stream power is less than at the crest.

Here, we analyze bedrock-stream incision and landscape evolution in a mountainous area of southern Spain by studying the ca. 300 ka to present history of a 42-km long reach of Río Andarax (Fig. 2). This reach of Río Andarax is fed by a 1270 km^2 catchment, and Río Andarax's total catchment area is 2027 km^2. The incision history of the Río Andarax drainage network was reconstructed on the basis of alluvial landform morphostratigraphy, calcrete crust development, and Th/U series-based geochronology. The incision history of the Río Andarax stream network is most simply and comprehensively explained as controlled by an incision wave (García, 2001). Additionally, temporal changes in relative stream-power distribution within the Río Andarax drainage basin are assessed, and provide

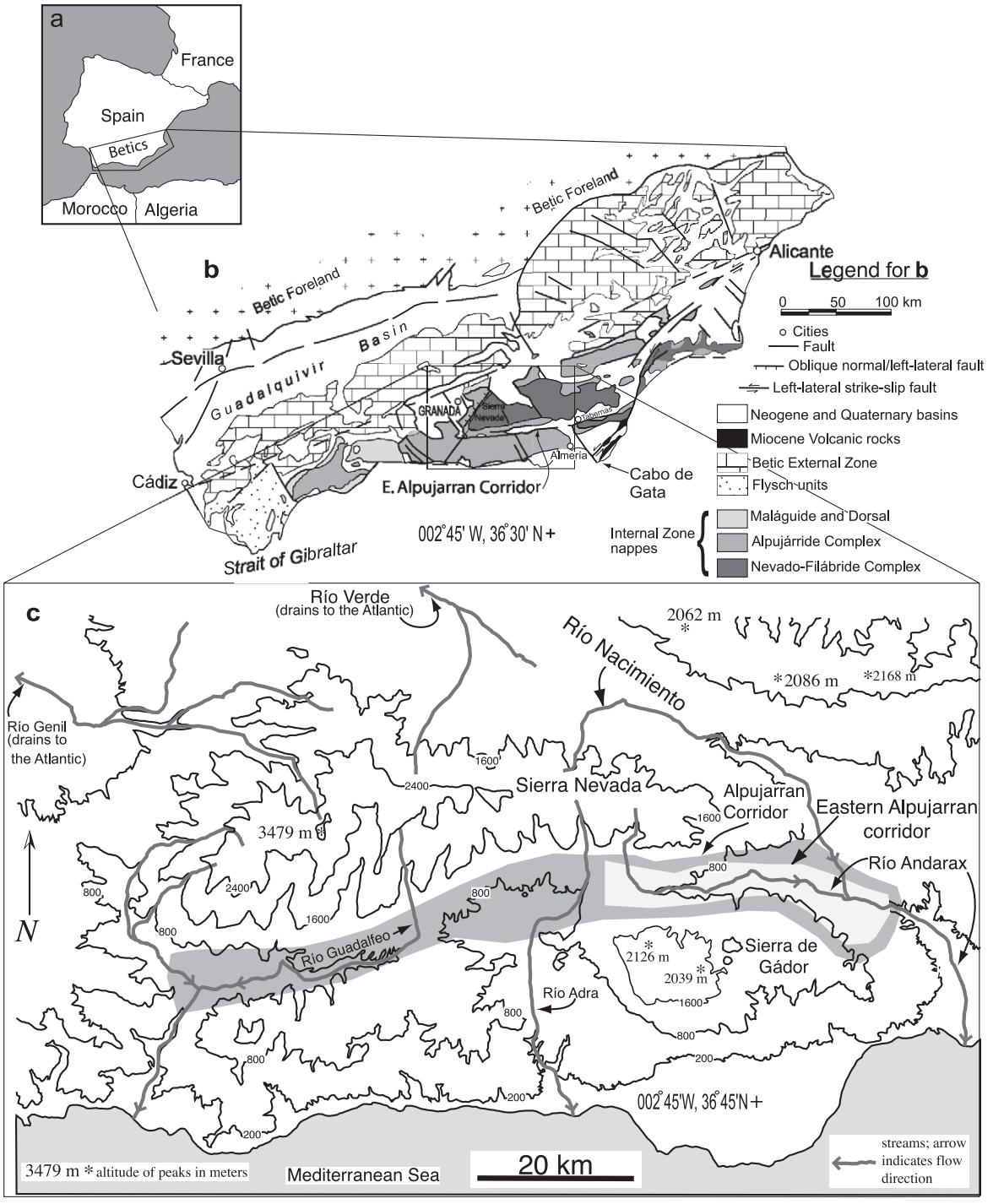

Fig. 2. Regional maps of the western Mediterranean and southern Spain. (a) Approximate location of the Betic Cordillera. (b) Simplified geologic map of the Betic Cordillera. The "Betic Foreland" is shown geographically rather than in terms of rock type. (c) Topographic map of the central part of the Betic Internal Zone. Contour lines are altitude in meters, and contour-line intervals vary.

insight regarding the effect of sediment supply and climate change on how incision waves move through bedrock stream networks. Thus, a historical–geologic approach is used to evaluate the time-dependent aspects of incision wave processes. This paper complements the prior quantitative studies that formulated the incision wave hypothesis (Anderson, 1994; Rosenbloom and Anderson, 1994; Safran, 1998) by: (1) providing field-geologic evidence that strongly suggests a history of bedrock stream entrenchment controlled by an incision wave; and (2) yielding new insight regarding factors controlling how incision waves move through bedrock stream networks.

1.3. Study area

The tectonically active Betic Cordillera is a topographic manifestation of the collision between the African and Iberian plates. It consists of E–W and NE–SW trending mountain ranges separated by lower lying sedimentary basins (Fig. 2). The altitude of Betic mountain-range summits is typically 1500–2500 m, and the altitudes of the highest peaks are greater than 3000 m (Fig. 2). The altitude of Betic basins varies from near sea level at the coast to 200–1000 m farther inland (Fig. 2). Betic basins were marine depocenters from late Miocene through Pliocene time, and were emergent by upper Pliocene/lower Pleistocene time (Sanz de Galdeano and Vera, 1992). Mid to late Quaternary tectonism in the Internal Zone of the Betic Cordillera (Fig. 2) consisted of regional uplift and localized faulting (e.g., Galindo Zaldívar et al., 1997; Sanz de Galdeano and López Garrido, 1999; García et al., 2003). Mid to late Quaternary rock uplift rates in the central part of the Betic Cordillera are on the order of 0.3–0.8 m/ka (Sanz de Galdeano and López Garrido, 1999; García et al., 2003).

The Alpujarran Corridor is one of several E–W trending structural corridors in the Betic Cordillera (Sanz de Galdeano, 1996). Most of the faults that define the Alpujarran Corridor formed during the Miocene time, westward displacement of the Internal Zone terrane relative to the Iberian craton (Sanz de Galdeano, 1996). The dominant structures of the Alpujarran Corridor are two 80-km long fault zones that are between 2 and 6 km apart, and that have accommodated between 40 and 75 km of right-lateral strike-slip separation, and up to 2 km of vertical separation (Sanz de Galdeano, 1996). Faults within these zones are typically 10 km long, strike 090–070°, and are mostly high angle to vertical (Sanz de Galdeano, 1996). This paper is based on the surficial geology of the eastern part of the Alpujarran Corridor (eastern Alpujarran Corridor, "EAC").

The EAC is a relatively long and narrow structural basin filled mostly with unconsolidated sediment that is bordered to the north and south by bedrock massifs. Physiographically, the EAC is a 30-km long and 4–6 km wide, E–W trending topographic trough bordered to the north and south by the highest mountain ranges in the Betic Cordillera (Fig. 2). Superimposition of the modern drainage network over basin-fill sediments led to development of rugged, steep topography within and adjacent to the EAC (Fig. 3). Quaternary fluvial denudation resulted in an erosional landscape characterized by prominent, high-level depositional surfaces, and multiple inset erosional surfaces (Figs. 3 and 4). Sediments comprising the depositional surfaces originated from tributaries to Río Andarax, which is the axial drainage of the EAC (Fig. 3). Topographic relief from the Río Andarax channel to adjacent mountainous crests is typically between 1000 and 1500 m. The dominant factor controlling landscape development in the EAC since the mid Quaternary is fluvial denudation driven by regional uplift (García et al., 2003). The rate of rock uplift in the EAC from ca. 500 ky to the present is between 0.3 and 0.7 m/ka (García et al., 2003).

The EAC lacks features indicative of fault-controlled stream and landscape development. Detailed morphological analyses, as well as field and air photo mapping, failed to identify fault-controlled knickpoints in streams, triangular facets ("flatirons") on mountain fronts, and fault-controlled lineaments (García, 2001; García et al., 2003). Deformation of Quaternary sediment in the EAC occurred along four faults within a 3-km^2 area (García et al., 2003) and one fault at the eastern end of the EAC (García, 2001) (Fig. 3). The maximum displacement on these faults is less than 10 m, and there is no evidence that active faulting within the EAC significantly affected mid Pleistocene to present stream or land-

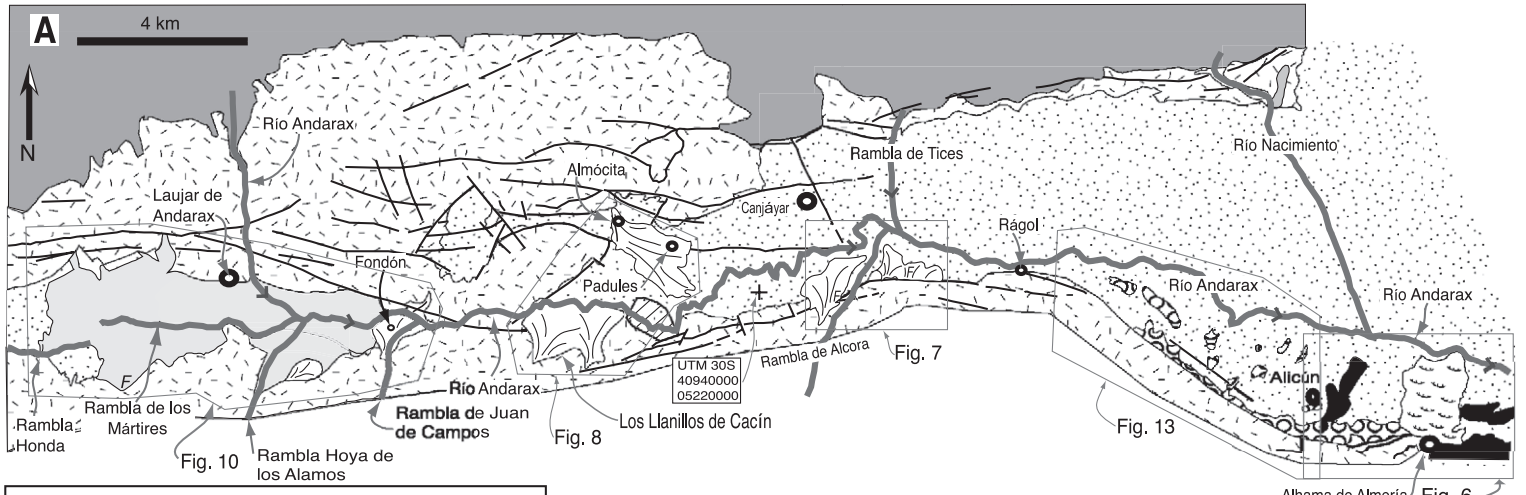
A
4 km
N
Río Andarax
Laujar de Andarax
Almócita
Canjáyar
Rambla de Tices
Río Nacimiento
Rágol
Fondón
Padules
Río Andarax
Río Andarax
UTM 30S
4094000
0522000
Rambla de Alcora
Fig. 7
Alcún
Rambla de los Mártires
Río Andarax
Rambla de Juan de Campos
Los Llanillos de Cacín
Fig. 13
Rambla Honda
Fig. 10
Rambla Hoya de los Alamos
Fig. 8
Alhama de Almería
Fig. 6

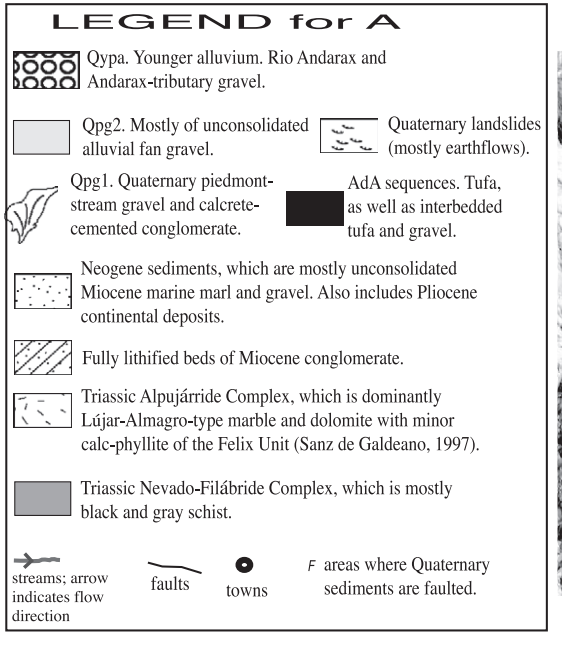
LEGEND for A
Qypa. Younger alluvium. Rio Andarax and Andarax-tributary gravel.
Qpg2. Mostly of unconsolidated alluvial fan gravel.
Quaternary landslides (mostly earthflows).
Qpg1. Quaternary piedmont-stream gravel and calcrete-cemented conglomerate.
AdA sequences. Tufa, as well as interbedded tufa and gravel.
Neogene sediments, which are mostly unconsolidated Miocene marine marl and gravel. Also includes Pliocene continental deposits.
Fully lithified beds of Miocene conglomerate.
Triassic Alpujárride Complex, which is dominantly Lújar-Almagro-type marble and dolomite with minor calc-phyllite of the Felix Unit (Sanz de Galdeano, 1997).
Triassic Nevado-Filábride Complex, which is mostly black and gray schist.
streams; arrow indicates flow direction
faults
towns
F areas where Quaternary sediments are faulted.

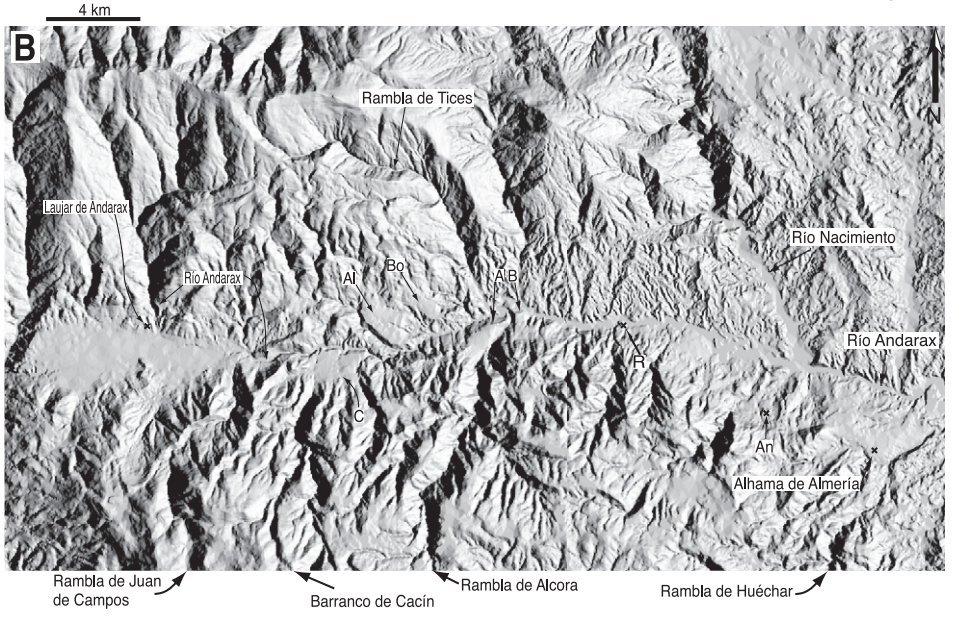
4 km
B
N
Rambla de Tices
Laujar de Andarax
Río Nacimiento
Río Andarax
Al
Bo
AlB
Río Andarax
F
C
An
Alhama de Almería
Rambla de Juan de Campos
Barranco de Cacín
Rambla de Alcora
Rambla de Huéchar

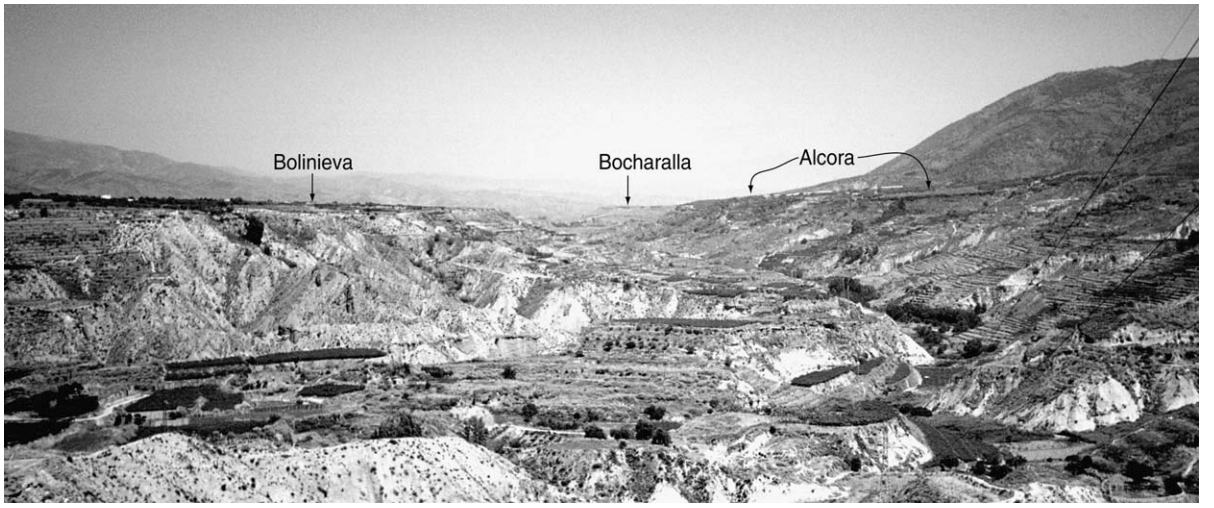

Fig. 4. View to the east from the Padules/Almócita Qpg1-landform surface. See Fig. 3 for the location of the labeled landforms.

scape development (García, 2001; García et al., 2003).

2. Methods and assumptions

2.1. Data collection

A 42-km long segment of Río Andarax was studied by mapping terrain along select reaches comprising a ca. 75-km^2 area. Mapping was conducted using 1:12,500 scale base maps. Paleodepositional environments were reconstructed through detailed sedimentologic logging and morphostratigraphic analyses of alluvial deposits (see the following section for details). Calcrete crusts on fluvial landform surfaces were evaluated using field characterization and petrographic analyses of thin sections. Soil and calcrete crust properties were used to correlate and estimate the ages of fluvial deposits and landforms, and also provided insight regarding landscape evolution (e.g., Alonso-Zarza et al., 1998).

Th/U series analyses of tufa-fossilized plant stems collected from alluvial sequences provided numeric age control for EAC Quaternary geochronology (García, 2001; García et al., 2003). The tufa samples were analyzed using α counting at the University of Southern California Geochemistry Laboratory. Analytical procedures used are described in Ku et al. (1990) and Ku (2000).

2.2. Interpretation of alluvial morphostratigraphy

Morphostratigraphic analysis of alluvial sediments was used to deduce paleo-relative-stream power in the Río Andarax stream network. This section outlines how the conceptual models of Bull (1979) and Bull (1990) were used to deduce patterns of paleostream power in the Río Andarax network on the basis of alluvial morphostratigraphy.

The quantitative component of Bull's (1979, 1990) models is available stream power (sensu Bagnold, 1973), which is time-dependent. The time-dependent nature of Bull's (1979, 1990) models makes them ideal for deducing paleohydrologic conditions in historical geomorphologic studies. For instance, the models presented Bull (1979, 1990) are the basis for morphostratigraphic analyses of fluvial stratigraphy in

Fig. 3. (A) Generalized geologic map of the eastern Alpujarran Corridor, modified from Sanz de Galdeano et al. (1991). Some Quaternary units are reinterpreted, and some faults are omitted for clarity. (B) Digital elevation model of Sierra Nevada, Sierra de Gádor, and the eastern Alpujarran Corridor. Illumination is from the east. Note the anomalously low-relief terrain south Laujar de Andarax (denoted by an "x"), which is known as "La Vega de Laujar". The fundamental basis of this paper is the surficial geology of La Vega de Laujar and the following areas: C, Los Llanillos de Cacín; Al, Almócita Qpg1; Bo, Bolinieva strath; A, Alcora Qpg1 complex; B, Bocharalla Qpg1 complex; An, town of Alicún; R, town of Rágol.

Table 1
Summary description of Quaternary map units

Map unit[a]	Map unit name	Sedimentology/morphostratigraphy	Additional notes
Qc	Quaternary cover	Quaternary cover. Includes colluvium, but is mostly terrain modified by human activity.	Mostly towns, orchards, and agricultural terraces.
Qpg3	Quaternary piedmont-stream gravel (youngest)	Fluvial terraces along Rambla de los Mártires, and along Río Andarax between Rambla de los Mártires and Rambla de Juan de Campos (Fig. 10). Qpg3 terrace treads are between 2 and 5 m above the Andarax and Mártires channels. The bases of Qpg3 deposits are not exposed. Qpg3 is unconsolidated, clast supported gravel, and sand. Gravel beds are massive, but are locally imbricated and stratified.	Qpg2 and Qpg3 treads merge near the headcut at the upstream end of Rambla de los Mártires (Figs. 5 and 10).
Qlst	Quaternary landslide with tufa blocks	Earthflows and slumps. Qlst is mostly earthflows consisting of blocks of tufa that are typically tens of cubic meters and up to hundreds of cubic meters in a 'matrix' of Miocene and Quaternary marl. A fossil plant stem collected from a tufa block in Qlst yielded an age of 354 ± 76 ky (Table 6), but in many localities Qlst are Holocene/Recent in age.	Active and inactive slope failures.
Qls	Quaternary landslide	Earthflows and slumps. Most common at the edges of the Bocharalla Qpg1 complex and the Alcora Qpg1 complex where streams have incised 50 m or more below the contact of Qpg1 and Miocene sediments (Fig. 7).	Active and inactive slope failures.
Qag	Quaternary axial-stream gravel	Qag sediments are poorly indurated to unconsolidated, well stratified and/or imbricated, clasts-supported gravel that is locally massive, and up to 7 m thick. Based on the unpaired nature of these terrace remnants, and on the great variability in their heights, Qag deposits are interpreted as complex response/minor strath terraces (sensu Bull, 1990).	Unpaired strath terraces.
Qtc	Quaternary true colluvium	Massive, poorly sorted deposits that comprise aprons and wedges at the bases of hillslopes. Locally graded to higher altitudes than the Qpg2 paleofluvial level.	
Qypa	Quaternary younger piedmont alluvium	Unconsolidated, colluvial and alluvial gravel, sand, and minor silt. The gravel is dominantly clasts of bluish-black Alpujárride marble and dolomite, and includes common fragments of caliche rubble. The clasts are dominantly angular to subangular, and include very minor amounts of sub-rounded and rounded clasts. Qypa sediments are active debris fan, alluvial fan, and alluvial-distributary channel deposits.	These sediment are "minor" or "complex response" deposits (sensu Bull, 1990; García, 2001).

Table 1 (*continued*)

Map unit[a]	Map unit name	Sedimentology/morphostratigraphy	Additional notes
Qyt	Quaternary younger tufa	Tan to gray, locally silty, and massive tufa. Rings sharply and distinctively when struck with a hammer. The deposits form arcuate outcrops that are tens of meters in length by ten to twenty meters wide, and bean shaped outcrops that are 10–100 m wide. Present slightly upslope and mostly downslope of faults. The age of these tufa deposits is inferred, and is based on landscape and stratigraphic position.	Probably formed as a result of groundwater discharge from faults and fractures.
Qpg2	Quaternary piedmont-stream gravel	Interbedded, clast-supported, stratified gravel, massive imbricated gravel, stratified pebble gravel, and massive silt (Fig. 12). Buried soils are commonly present within Qpg2 sequences. The bases of Qf2 deposits are not exposed, and the maximum exposed thickness of Qpg2 is 18.6 m, along Rambla Honda, which is west of the Río Andarax watershed (Figs. 3, 5, and 10).	Buried soils are commonly present within Qpg2 sequences. Inset into Qpg1 and is inset into by Qpg3.
Qpg1	Quaternary Piedmont-stream gravel (oldest)	Lenticular beds of crudely sorted, clast-supported, massive and stratified, subangular gravel and silty-sand. The width of lenticular beds varies from 1 to 12 m, and their thickness varies from 0.2 to 1.5 m. Clasts in these beds are typically less than 5 cm, but as large as 18 cm. The lenticular beds are interbedded and interfingered with beds consisting of poorly sorted, matrix supported, massive, subangular gravels supported within a sandy-silt matrix. These matrix-supported beds are laterally continuous across outcrops as wide as 15 m.	Buried soils are present within this and most Qpg1 deposits. All Qpg1 deposits dip gently toward Río Andarax and away from EAC mountain fronts.
Qt	Quaternary tufa	Massive tufa beds that are typically between 0.4 and 0.7 m thick, but up to 2 m thick, and are locally fossiliferous. Fossils in the tufa are cylindrical, elongate plant stems that have diameters of a few mm and lengths of a few centimeters. The fossil plant stems are typically horizontal, and their trends are parallel to paleotransport directions inferred from bedding attitude.	Analyzed in detail in García et al. (2003). Numeric age based on U/Th dates is coincident with oxygen isotope Stage 8 (Garcia et al., 2003). Occupy the same landscape position as Qpg1.
Qtd	Quaternary tufa/debris flow deposits	Decimeter to meter-thick, locally lenticular beds of tufa and fossiliferous tufa as in Qt. Tufa beds are interlayered with silt and sand, as well as stratified and massive gravel. The sequences are typically 10–20 m thick, and are capped by tufa, and the surfaces of landforms underlain by Qtd sequences are formed by tufa. Qtd sequences overlie smooth unconformities cut into Mcs and PQc, and dip gently away from the local Sierra de Gádor mountain front.	Analyzed in detail in García et al. (2003). Numeric age based on U/Th dates is coincident with oxygen isotope Stage 8 (Garcia et al., 2003). Occupy the same landscape position as Qpg1.

[a] Map units are listed from youngest to oldest. Ages are relative and inferred from landscape position.

many recent investigations (e.g., Harvey, 1990; Merritts et al., 1994; Harvey et al., 1995; Personius, 1995; Pazzaglia et al., 1998; Harvey et al., 1999a,b; Pazzaglia and Brandon, 2001).

Because the models of Bull (1979, 1990) are time-dependant, here we specify a timescale for evaluating paleo-relative-stream power. In tectonically active areas, fluvial strath formation occurs when available power equals critical power (Bull, 1979, 1990). Accordingly, we assume that fluvial straths overlain by oxygen isotope Stage 8 (OIS8)-time gravels indicate that the flux of sediment into Río Andarax tributaries was about the same as the flux of sediment out of Río Andarax tributaries during OIS8 (303–245 ka, Imbrie et al., 1984). Fluvial fills form when critical power exceeds available power (Bull, 1979, 1990), and we assume OIS8-time fills indicate that, between ca. 303 and 245 ka, more sediment was delivered to the channels of Río Andarax tributaries than they were able to transport.

2.3. Definition of a bedrock-channel stream based on process

The EAC is underlain largely by unconsolidated, Miocene-age sediment, and most reaches of the Río Andarax and its tributaries flow over unconsolidated sediment. In this section, the rationale behind analyzing the Río Andarax and its tributaries as a bedrock-channel stream network is explained. The term "bedrock-channel stream" usually refers to streams flowing over fully lithified rock. Here, it is proposed that streams incising through unconsolidated substrate respond to external forcing factors (like tectonically induced base-level fall) in the same way as streams incising through fully lithified bedrock. Sediment size and supply rate are a more significant control on bedrock-stream-incision related dynamics than rock type (Sklar and Dietrich, 1998), suggesting that channel substrate is not the definitive characteristic of a bedrock stream.

One defining attribute of bedrock-channel streams is that available stream power is always sufficient to transport all sediment delivered to the channel (Seidl and Dietrich, 1992; Tinkler and Wohl, 1998; Pazzaglia et al., 1998). Sediment transport in such streams is said to be "detachment limited" (Howard, 1994). The Río Andarax stream valley and Andarax tributary-stream valleys east of Fondón (Fig. 3) lack floodplains, alluvium (other than active-channel gravel), and stream terraces younger than about 245 ka (García, 2001; García et al., 2003). This indicates that since 245 ka, available stream power exceeded critical power in streams east/downstream of Fondón (Bull, 1979, 1990; Fig. 3), and that fluvial processes have been detachment limited (cf. Seidl

Table 2
Altitude and height-above-channel data for AdA sequences and Qpg1 deposits

	Alhama de Almería sequence I (Qtd)[a]	Alhama de Almería sequence II (Qt)[a]	Alhama de Almería sequence east of Alicún (Qtd)[a]	Bocharalla Qpg1 complex[a]	Almócita Qpg1[a]	Los Llanillos de Cacín Qpg1[a]	Rambla de Juan de Campos Qpg1[a]
Distance from river mouth	24.1 km	24.8–25.1 km	28.8 km	41.4–42.9 km	50.0–50.8 km	52.9–55.4 km	58.6–60.0 km
Plan-view distance of data (um) from Río Andarax's Channel	375 m	144–250 m	> 500 m	194–338 m	263–325 m	75–81 m	–
Altitude of the base of the deposit	300 m	300 m	395 m[b]	590 m	710–715 m	710–765 m	<780–<800
Height of base of the deposit above Río Andarax	95 m	65 m	155 m[b]	160–145 m	145–135 m	25–80 m	<0 (base not exposed)

[a] Localities shown in Fig. 3.
[b] Calculated by projecting from the axial-streamward edge of the deposit to the present-day position of the Río Andarax channel using the slope of the landform tread underlain by this Qtd deposit.

and Dietrich, 1992). Similarly, the prevalence of oxygen isotope Stage 8-time fluvial straths east of Almócita (García, 2001; García et al., 2003; Fig. 3) indicates that most of the Andarax network was vertically incising into Miocene and Neogene-age unconsolidated sediments before OIS8 (cf. Bull, 1979, 1990). Although the Río Andarax network in the EAC is developed mostly in unconsolidated sediment, detachment-limited fluvial processes have prevailed east of Almócita since before 303 ka and east of Fondón since ca. 245 ka. Therefore, although it flows mostly over unconsolidated sediment, the last several hundred thousand years of Río Andarax stream-network development were dominated by detachment-limited processes, like those prevalent in conventional bedrock-channel streams flowing over fully lithified rock.

3. Pre-Quaternary geology of the eastern Alpujarran Corridor and surrounding mountains

This section describes the pre-Quaternary geology of the EAC, which is necessary for establishing the provenance of fluvial sediments, and for characterizing the geologic setting of the study area.

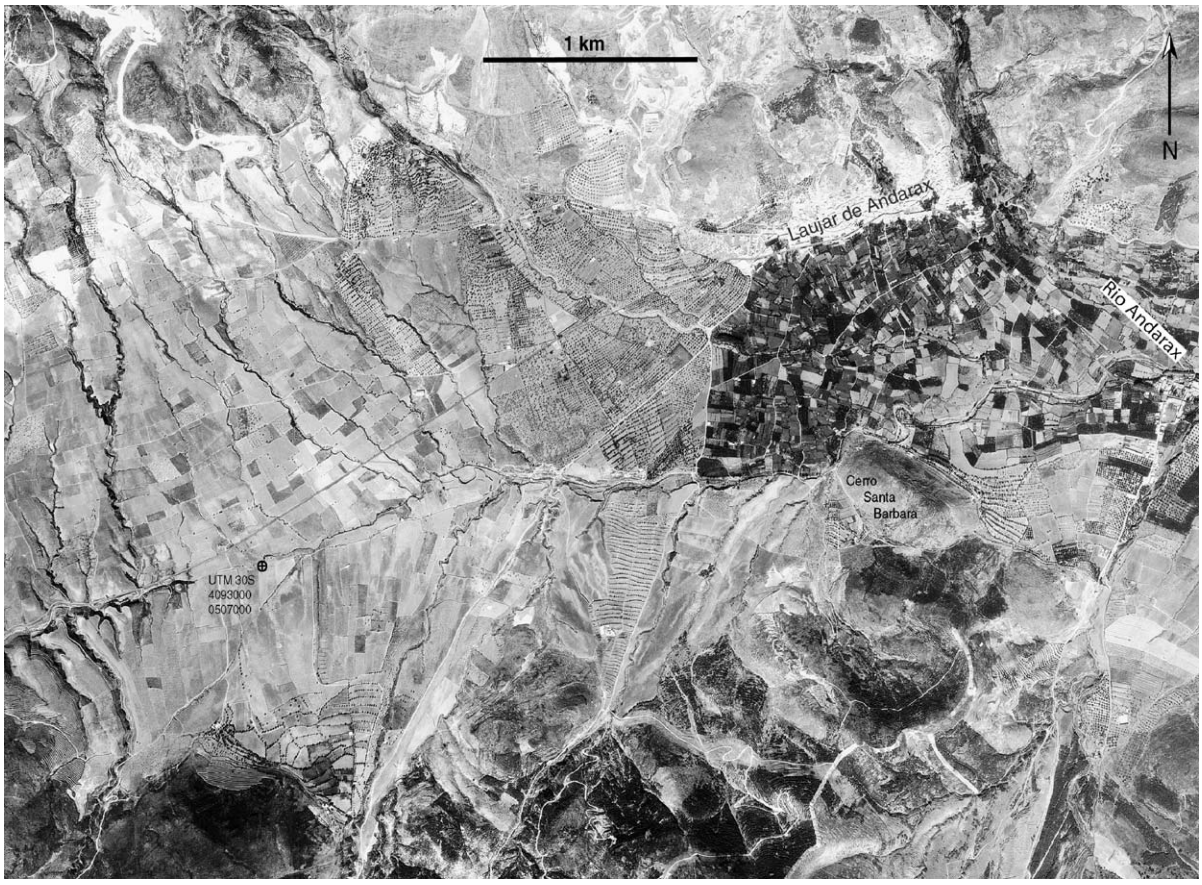

Fig. 5. Aerial photograph of the western end of the EAC, which is dominated by coalesced alluvial fans. The deeply incised stream at the left is Rambla Honda, which is not part of the Andarax stream network, and drains to the west into Río Adra (Fig. 2). Río Andarax is the large stream at the east edge of Laujar de Andarax; it trends SSE north of Laujar and it trends SE south of Laujar. Rambla de los Mártires is the E trending stream in the center of the western part of La Vega de Laujar. Notice that streams (including Rambla de los Mártires) are incised across the entire lengths of the alluvial-fan surfaces. Photo used with permission from the Instituto Geográfico Nacional-Centro Nacional de Información Geográfica de España.

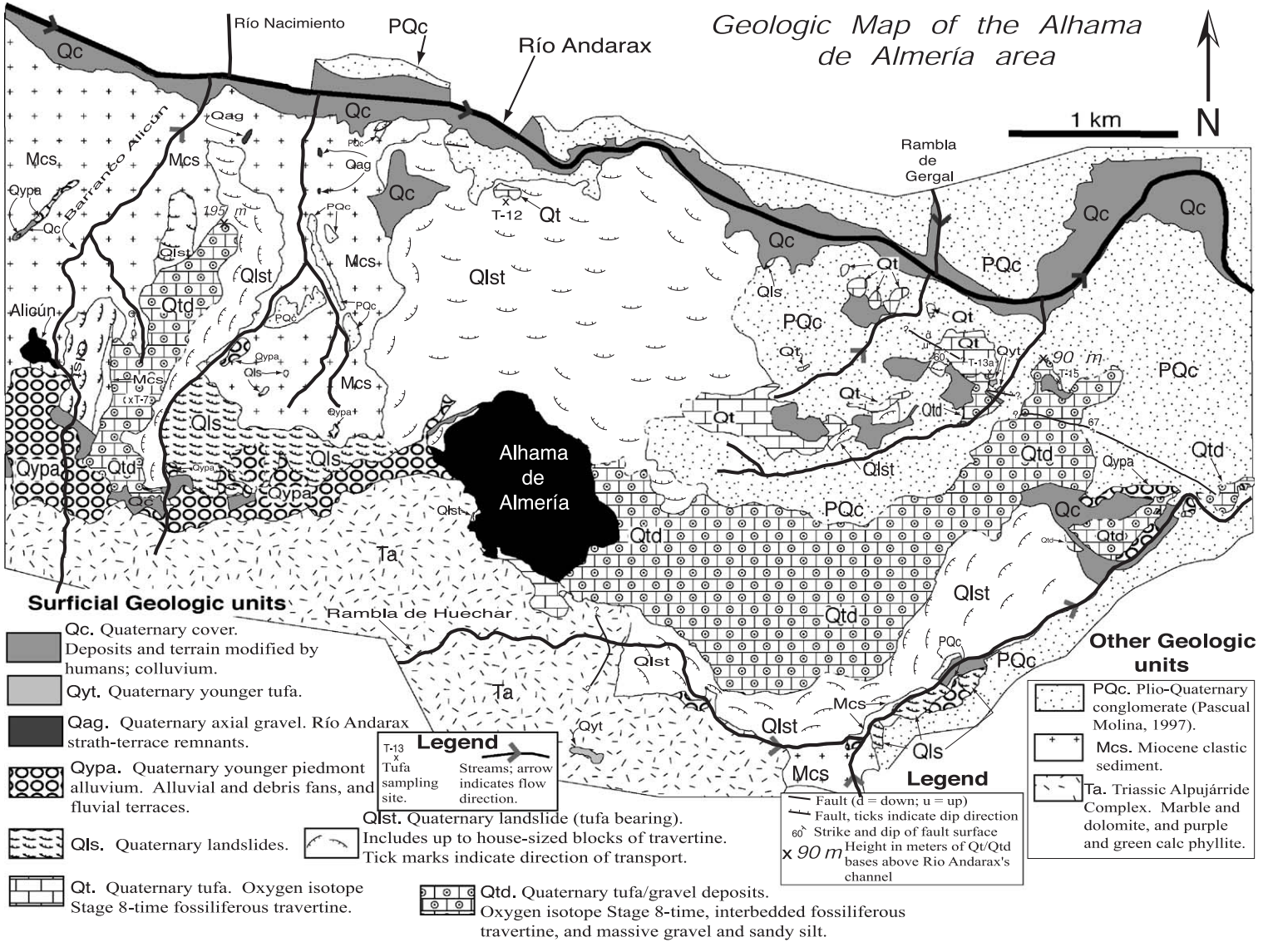

Fig. 6. Geologic map of the Alhama de Almería environs. Qc adjacent to Río Andarax is agricultural terraces.

3.1. Metamorphic basement

Rocks exposed in mountain ranges adjacent to the Alpujarran Corridor and basement rocks of the Alpujarran Corridor are part of the Betic Internal Zone nappe sequence (Sanz de Galdeano, 1997) (Fig. 2). The Sierra de Gádor, which is adjacent to and south of the EAC, is almost entirely underlain by marble and dolomite of the Alpujárride Complex nappe (Figs. 2 and 3; Sanz de Galdeano, 1997). The Sierra Nevada, which is adjacent to and north of the EAC, is underlain largely by pelitic, high-grade metamorphic rocks of the Nevado-Filábride Complex nappe (Figs. 2 and 3). The southern flank of the Sierra Nevada is locally formed by Alpujárride Complex rocks (Fig. 3).

3.2. Neogene basin-fill sediments

Miocene basin-fill sediments in the EAC (Mcs; Figs. 2 and 3) are unconsolidated marl, sand, gravel (Sanz de Galdeano et al., 1991), and minor amounts of tufa (García, 2001). Tufa beds are 1–3 m thick and are typically present only in the upper part of Mcs sequences. Near the town of Alhama de Almería, basin-fill sediments are dominantly Plio-Quaternary conglomerate and gravel (map unit PQc). PQc is fanglomerate, *sensu stricto*, and the sediments are substrata dissected by the present-day fluvial network (García, 2001; García et al., 2003). PQc is mostly moderately indurated sand and gravel, with minor unconsolidated sand and gravel. North of highway N-324 and south of Río Andarax, PQc is completely indurated conglomerate. PQc deposits are up to 100 m thick, and their base is not exposed in the mapped area. Based on stratigraphic relationships and regional correlations, Pascual-Molina (1997) inferred these sediments to be uppermost Pliocene and lowermost Pleistocene in age.

4. Mapping results

Field observations and field-mapping results are presented in this section. First, the physiography of the EAC is described. In following subsections, the morphostratigraphy of EAC Quaternary alluvial stratigraphy is described and interpreted. The emphasis of the descriptions is on the morphostratigraphy of fluvial deposits and landforms that are most useful for deducing paleo-relative-stream power in the EAC. Summary descriptions of Quaternary map units are presented in Table 1.

4.1. Physiography of the EAC

East of Fondón (Fig. 3), EAC Quaternary landforms are underlain by calcretized gravel (Quaternary piedmont gravel "Qpg1", described in detail below and Table 1), and by tufa and interbedded alluvial sediments ("AdA sequences"; which consists of the Qtd and Qt map units, also described in detail below and Table 1). The anomalously low-relief surfaces of Qpg1

Table 3
Relative stream power of select Río Andarax tributaries during AdA sequence/Qpg1 time deduced from morphostratigraphy

AdA sequence/Qpg1 feeder streams, and reference map[a]	Relative stream power during AdA sequence/Qpg1 time	Distance of confluence with Río Andarax from the Andarax river mouth
Rambla de Huechar, Fig. 6	available power = critical power	21 km
Barranco Alicún, Fig. 6	available power = critical power	29.5 km
Barranco de la Fuente, Fig. 13	available power>critical power	31 km
Barranco de Colomina, Fig. 13	available power>critical power	36.5 km
Rambla de Alcora, Fig. 7	available power = critical power	45 km
Barranco del las Eras, Fig. 8	available power = critical power	49 km
Barranco del Bosque, Fig. 8	available power = critical power	51 km
Barranco del Pilar, Fig. 8	available power < critical power	53 km
Barranco de Cacín, Fig. 8	available power < critical power	55 km
Rambla de Juan de Campos, Fig. 10	available power < critical power	59 km
Barranco del Infierno, Fig. 10	available power < critical power	59 km
Rambla Hoya de los Alamos, Fig. 10	available power < critical power	62 km

[a] Also see Fig. 3 for the location of streams and maps.

and AdA-sequence landforms visually dominate the EAC landscape, which otherwise consists of exhumed and dissected Neogene sediments (Fig. 3). From selected vantage points (Fig. 4), Qpg1 and AdA-sequence landform surfaces are unquestionably a paleovalley floor and/or a piedmont flanking a paleovalley floor, and are at the same paleoalluvial level. Depth of stream incision below AdA sequences and Qpg1 is listed in Table 2. Qpg1 deposits adjacent to Rambla de Alcora (Fig. 3) are temporally correlative to the AdA sequences (García et al., 2003). Chronostratigraphic correlation of all EAC Qpg1 deposits to each other and to the AdA sequences is established in a following section using calcrete-crust morphology, and by analyses based on regional models of climatically driven cycles of fluvial aggradation and degradation.

The geomorphic character of the EAC west of Fondón (Fig. 3) is markedly different from the rest of the EAC. It is dominated by low relief, undissected, and coalesced alluvial surfaces. Streams are incised a few meters to about 10 m below alluvial surfaces (Figs. 3 and 5).

4.2. Description and interpretation of the morphostratigraphy of the Alhama de Almería sequences

At the eastern end of the Alpujarran Corridor, on the Sierra de Gádor piedmont near the towns of Alhama de Almería and Alicún, there are sequences consisting of tufa, fluvial deposits, and debris-flow deposits (García et al., 2003; "AdA sequences"; map units Qtd and Qt in Fig. 6). These deposits are critical to this study because Th/U-series analyses of fossil plant stems collected from AdA sequences provide numeric age control for EAC Quaternary geochronology (García et al., 2003). They are also important because they locally define the single paleoalluvial level in the EAC east of Almócita.

AdA sequences were deposited by a fluvial and/or alluvial fan system during OIS8 (García, 2001; García et al., 2003). Qtd deposits are relatively thin and overlie straths cut in EAC basin-fill sediments. The straths were cut by the Barranco Alicún and the Rambla de Huechar (García et al., 2003; Fig. 6 and Table 3). The association of relatively thin fluvial gravels over fluvial straths indicates streams were at the threshold of critical stream power when deposition took place (Table 3; García et al., 2003; cf. Bull, 1979, 1990; Pazzaglia et al., 1998; Pazzaglia and Brandon, 2001). After Qt and Qtd were deposited, incision by Río Andarax and its tributaries has been largely uninterrupted (García et al., 2003). The few alluvial sediments present below the Qtd/Qt paleoalluvial level are minor complex-response degradation terraces (García et al., 2003) that reflect fluvial network response to intrinsic factors (Bull, 1990).

4.3. Description and interpretation of Quaternary piedmont gravel (Qpg1) morphostratigraphy and map pattern

Areally, the most extensive surficial geologic deposit in the EAC is older Quaternary piedmont gravel (Qpg1), which consists of alluvial gravels capped by calcrete crusts. Qpg1 sediments were deposited by Río Andarax tributaries, and landforms underlain by Qpg1 locally form the Sierra Nevada and Sierra de Gádor piedmont (García, 2001; García et al., 2003). Qpg1 deposits are lithostratigraphically correlative, but their morphostratigraphy varies (García, 2001; García et al., 2003).

East of Almócita (Fig. 3), Qpg1 deposits overlie fluvial straths (Garcia, 2001; García et al., 2003; Figs. 7–9). The association of relatively thin fluvial gravels over fluvial straths (Fig. 9), indicates streams were at the threshold of critical stream power when deposition took place (Table 3) (Bull, 1979, 1990; Pazzaglia et al., 1998; Pazzaglia and Brandon, 2001). Qpg1 feeder-stream valleys east of Almócita lack alluvium other than active channel gravel. This indicates that available power has exceeded critical power in EAC streams east of Almócita since Qpg1 deposition.

West of Almócita and east of Fondón (Fig. 3), Qpg1 deposits comprise alluvial fans (Figs. 8 and 10), and the thickness of these alluvial fan deposits locally

Fig. 7. Geologic map of the Bocharalla Qpg1 complex and Alcora Qpg1 complex. The Alcora Qpg1 complex is fan shaped in plan view, but otherwise its morphostratigraphy is strath-terrace like. The western lobe of the Bocharalla Qpg1 complex is a strath terrace. See Table 1 and text for detailed explanation of map units.

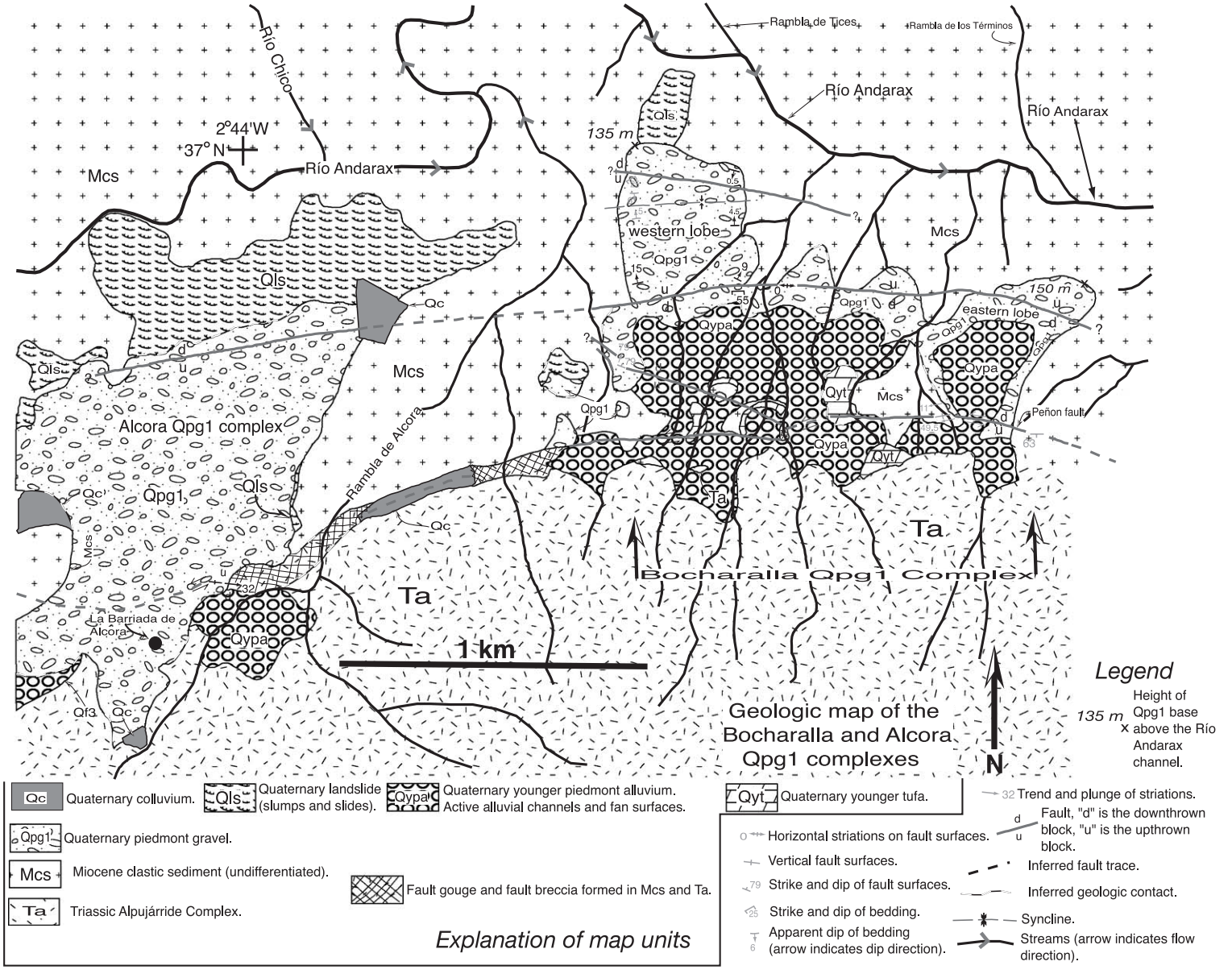
Río Chico
2°44'W
37° N
Río Andarax
Mcs
Qls
Qc
Alcora Qpg1 complex
Qpg1
Rambla de Alcora
Ta
1 km
La Barriada de Alcora
Qypa
Qf3
Rambla de Tices
Rambla de los Términos
135 m
western lobe
150 m
eastern lobe
Qyt
Peñon fault
Bocharalla Qpg1 Complex
Geologic map of the Bocharalla and Alcora Qpg1 complexes
N
Legend
Height of Qpg1 base above the Río Andarax channel.
Quaternary colluvium.
Quaternary landslide (slumps and slides).
Quaternary younger piedmont alluvium. Active alluvial channels and fan surfaces.
Quaternary younger tufa.
Quaternary piedmont gravel.
Miocene clastic sediment (undifferentiated).
Triassic Alpujárride Complex.
Fault gouge and fault breccia formed in Mcs and Ta.
Explanation of map units
Trend and plunge of striations.
Fault, "d" is the downthrown block, "u" is the upthrown block.
Horizontal striations on fault surfaces.
Vertical fault surfaces.
Strike and dip of fault surfaces.
Strike and dip of bedding.
Apparent dip of bedding (arrow indicates dip direction).
Inferred fault trace.
Inferred geologic contact.
Syncline.
Streams (arrow indicates flow direction).

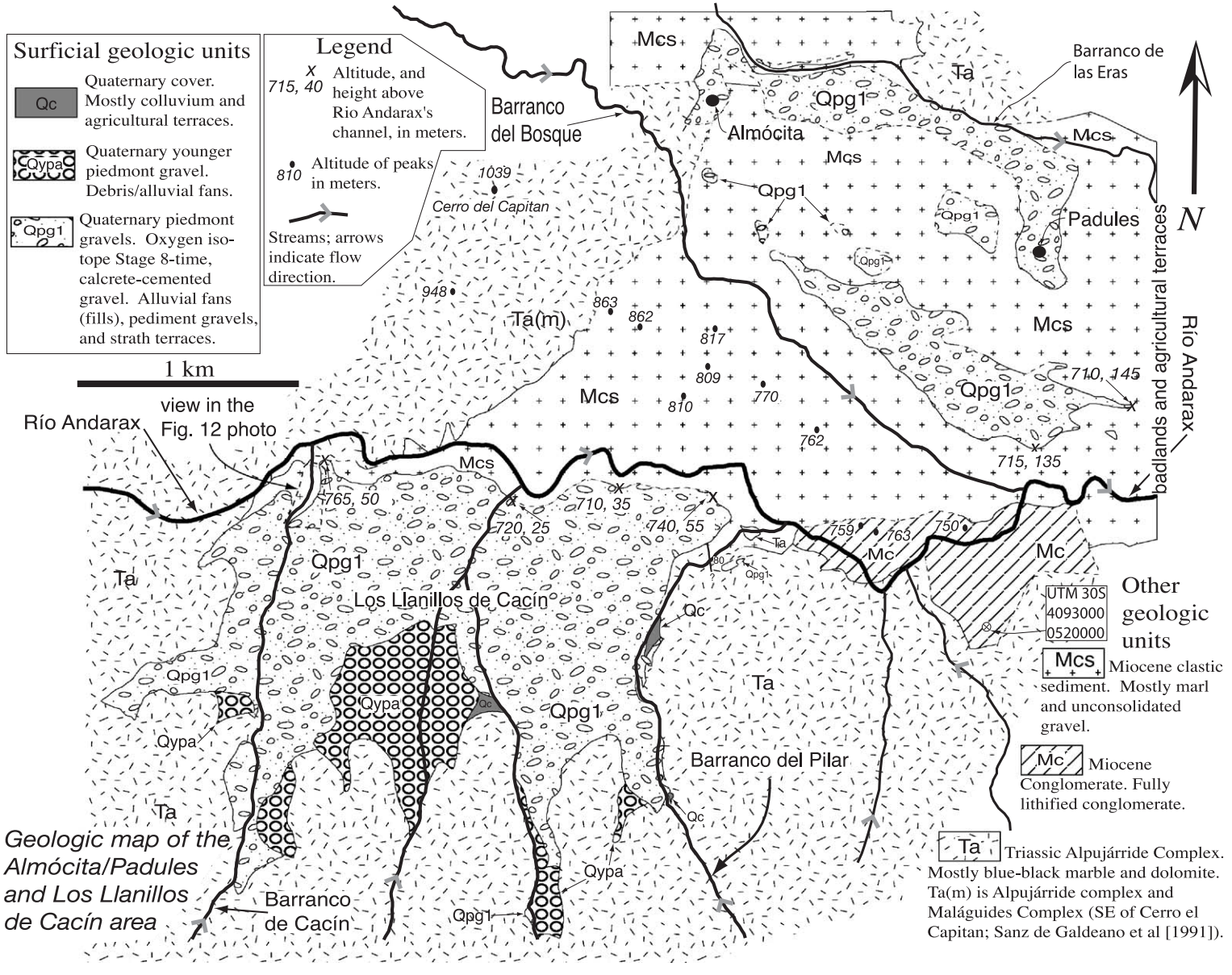

Geologic map of the Almócita/Padules and Los Llanillos de Cacín area

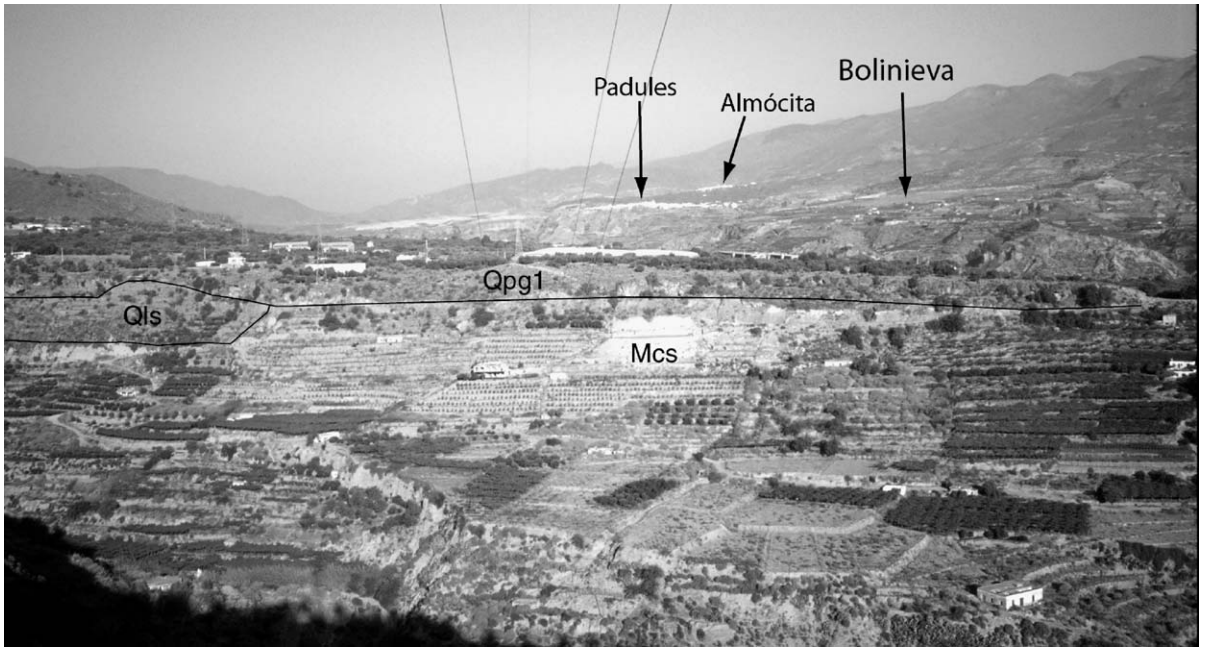

Fig. 9. View to the west of the Alcora Qpg1 complex from the Bocharalla Qpg1 complex. The Qpg1–Mcs contact is drawn in black. The arrows indicate the locations of the towns of Padules, Almócita, and the Bolinieva strath.

exceeds 35 m. Qpg1 deposits at Los Llanillos de Cacín overlie irregular unconformities (Figs. 8 and 11), indicating that available power exceeded critical power when deposition occurred (Table 3; Bull, 1979, 1990). In the Fondón area (Fig. 10) Qpg1 is up to 28 m thick, and the bases of these deposits are below the present altitude of streams in the Río Andarax network. This strongly suggests that critical power exceeded available power when these Qpg1 fans were deposited (Table 3; cf. Bull, 1990). No alluvium other than active channel gravel is present in Qpg1 feeder streams between Almócita and Fondón, which indicates that available power exceed critical power since Qpg1 deposition.

West of Fondón, Qpg1 deposits are exposed in the apices of alluvial fans underlain mostly by Qpg2. These Qpg1 deposits are up to 12 m thick and are buried and inset into by Qpg2 deposits (Figs. 10 and 12; García, 2001). The most notable aspect of Qpg1 morphostratigraphy west of Fondón is that the present-day fluvial network has not incised below the bases of the deposits. This strongly suggests that critical power exceeded available power when they were deposited (Table 3; cf. Bull, 1990).

4.3.1. Bolinieva area

Sanz de Galdeano et al. (1991) mapped a Pleistocene alluvial fan northwest of the Alcora Qpg1 complex and northeast of Padules (Figs. 3, 4, and 9). The area is an orchard known as Bolinieva, and it is a low-relief-surface landform that is very similar to the Qpg1 landforms in the Padules and Almócita environs. The Bolinieva surface is probably part of the same paleovalley floor underlain by other Qpg1 deposits (Figs. 4 and 9). However, the surface of the Bolinieva landform is heavily cultivated, and there is

Fig. 8. Geologic map of the Almócita and Padules environs and of Los Llanillos de Cacín. The large Qpg1 deposit south of Padules is fan-like in plan view, but otherwise its morphostratigraphy is strath-terrace like. Although the Padules/Almócita (N of Río Andarax) Qpg1 deposits overlap with Los Llanillos Qpg1 deposits (S of Río Andarax) in a Río Andarax frame of reference, they are separated by a NW trending ridge (note the elevation of peaks shown on the map; also see Fig. 3). The reach of Río Andarax in Mc is a vertical to sub-vertical walled bedrock gorge.

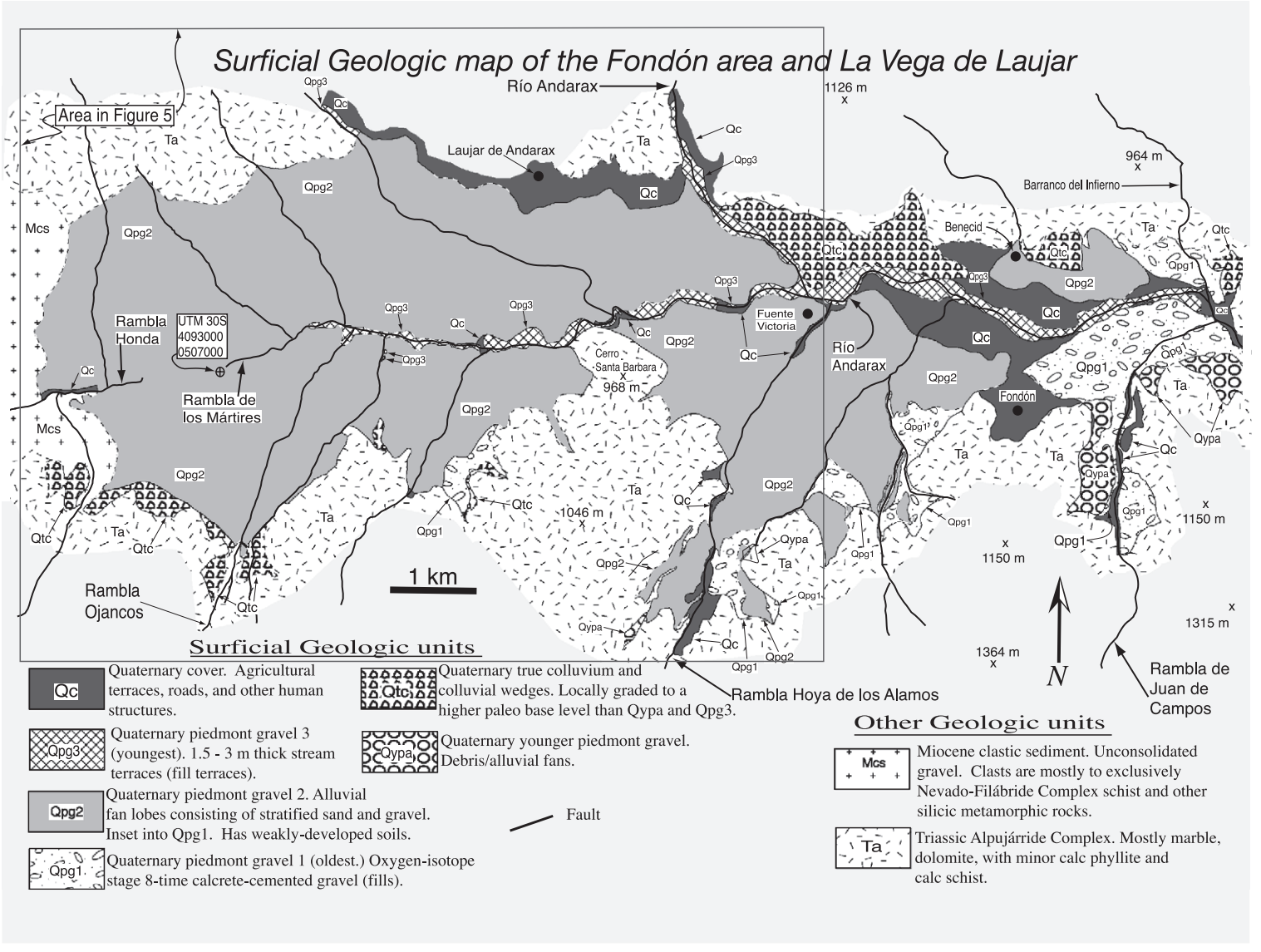

Fig. 10. Geologic map of La Vega de Laujar, Fuente Victoria, and Fondón area. The western boundary of the Andarax watershed in the EAC is between Rambla Honda and Rambla de los Mártires.

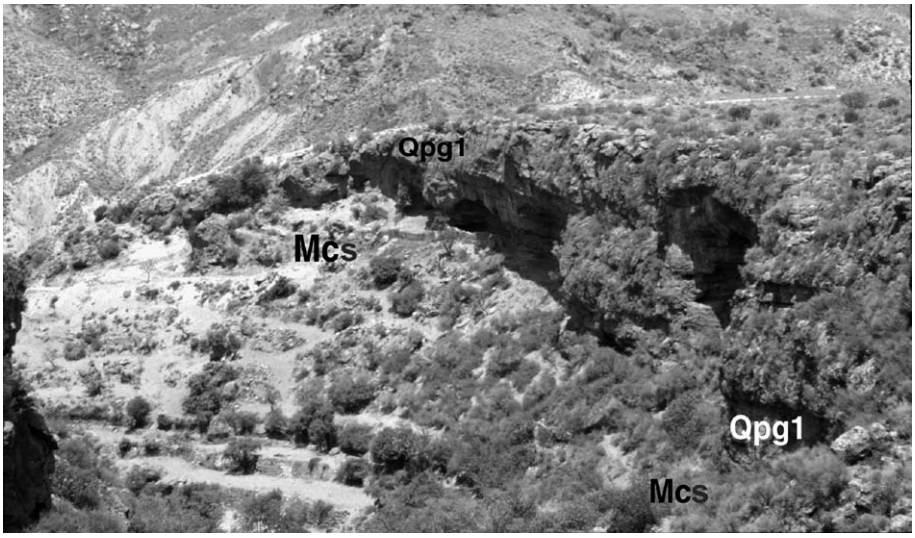

Fig. 11. View to the northeast across Barranco de Cacín near the western toe of the Los Llanillos Qpg1 alluvial fan (see Fig. 8 for location). At this outcrop, Qpg1 is a paleochannel fill. It is >20 m thick at the far right of the photo (its base is not exposed) and is 8–10 m thick at the left side of the photo.

insufficient exposure and/or preservation of Qpg1 gravels for morphostratigraphic analyses. The low-relief surface of the Bolinieva area landform strongly suggests that it is a fluvial strath cut in Miocene sediment (mostly marl; Garcia, 2001).

4.4. Surficial geology of the Íllar and Huécija environs (the EAC between the towns of Alicún and Rágol)

The geology of the part of the EAC described in this subsection is critical because it is the only part of the

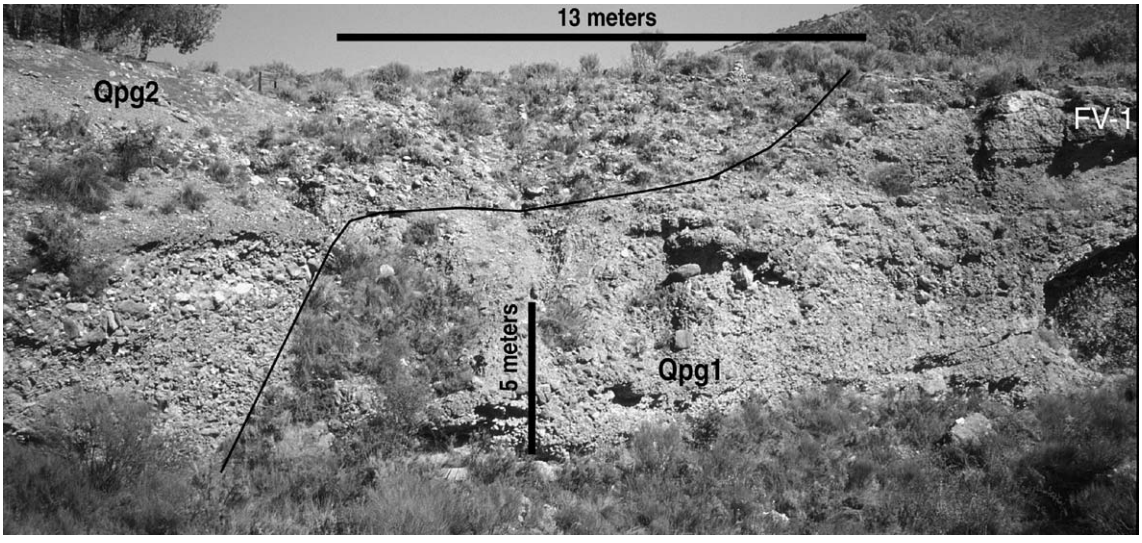

Fig. 12. View to the east of a Qpg1–Qpg2 contact on a Rambla Hoya de los Alamos stream bank. Note that Qpg2 is a fill; it is in buttress unconformable contact with Qpg1. Calcrete sample FV-1 was collected from the fully lithified calcrete bed labeled "FV-1", approximately 3 m south of the southern edge of the photo.

EAC where the Qpg1/AdA sequence paleoalluvial level is not present along a substantially long reach of Río Andarax (Fig. 3). North of Río Andarax, the Sierra Nevada piedmont between the towns of Alicún and Rágol (Fig. 3) consists of badlands formed in unconsolidated Miocene sediment. South of Río Andarax, the Sierra de Gádor piedmont between the towns of Alicún and Rágol is dominated by Río Andarax and Río Andarax-tributary minor straths (sensu Bull, 1990; García, 2001; Qag and Qypa, Fig. 13; Table 1). The straths are at lower levels and lower altitudes than the paleoalluvial level recorded by Qpg1 and the AdA sequences (García, 2001; Fig. 13).

4.4.1. Implications of the surficial geology of the Íllar and Huécija environs

The area between Rágol and Almócita (Fig. 3), which includes Íllar and Huécija environs (Fig. 13), is the only part of the EAC where deposits and landforms denoting the Qpg1/AdA sequence paleoalluvial level is not present (Fig. 3; García, 2001). The absence of Qpg1/AdA-sequence paleoalluvial level landforms can be explained in two ways. One explanation is that they were never present, because available stream power exceeded critical stream power during Qpg1/AdA-sequence time, and tributaries were incising vertically in response to tectonically induced base-level fall (Bull, 1979, 1990). Another possible explanation is that Qpg1/AdA sequence paleoalluvial landforms were deposited but are not preserved. The first explanation is favored because no factors were recognized that make preservation of Qpg1 landforms less likely in the area between Rágol and Almócita than in other parts of the EAC. For instance, strath terraces below the Qpg1/AdA sequence paleoalluvial level dominate the Sierra de Gádor piedmont in the Íllar and Huécija environs (Fig. 13). This suggests that local factors controlling landscape stability inherently favor preservation of alluvial landforms.

Additionally, calcrete crusts inhibit lateral stream incision, and streams incised into calcrete-crusted landforms are commonly restricted to narrow stream-channel valleys (Harvey, 1987). Because strath formation requires lateral incision (Bull, 1990; Pazzaglia and Brandon, 2001), the fluvial straths in the Íllar-Huécija area (Fig. 13), strongly suggest that extensive calcrete-crusted landforms like those underlain by Qpg1 were never present. The most likely explanation for the absence of a Qpg1/AdA sequence paleoalluvial level in the Íllar and Huécija area is that available stream power exceeded critical stream power during Qpg1/AdA-sequence time, and Río Andarax tributaries were incising vertically (Table 3).

Another factor that may have precluded formation of landforms at the Qpg1/AdA sequence paleoalluvial level between Rágol and Almócita is the distribution of stream catchment area. Stream catchment area can be a fundamental control on the distribution of available stream power (Safran, 1998), because greater catchment area equates to greater available stream power. The catchment area of Río Andarax does not increase significantly in the vicinity of Íllar and Huécija (Fig. 14). Therefore, relatively high available stream power due to an anomalously large increase in catchment area can be ruled out as the reason for the absence of OIS8-time paleoalluvial level in the Íllar and Huécija area.

4.5. Qpg2 deposits

The westernmost EAC valley floor is dominated by coalesced alluvial fans that consist mostly of Qpg2 deposits (Figs. 5 and 10; Table 1). This area is known as the "Vega de Laujar" and the alluvial fans that comprise the valley floor are referred to as the "Vega de Laujar fans". At Rambla Hoya de los Alamos, Qpg2 is inset into Qpg1 (Figs. 10 and 12). The bases of Qpg2 deposits are not exposed, and the maximum exposed thickness of Qpg2 is 18.6 m. Feeder streams are incised below Vega de Laujar fan surfaces across the entire lengths of the fans ("through trenched fans" sensu Harvey, 1990; Fig. 5).

Surfaces underlain by Qpg2 are heavily cultivated, and although it is not possible to make detailed soil profile characterizations, some assessment of soil development is possible. Carbonate accumulation features are weakly developed in Qpg2 soils. The only evidence for carbonate accumulation is effervescent reaction to HCl. It is possible that agricultural activity obliterated Stage I carbonate accumulation features (like carbonate filaments) on the cultivated Qpg2 surfaces. However, Stage II carbonate accumulation features include continuous coatings on tops and bottoms of clasts and the presence of nodules (Machette, 1985). It is unlikely that agricultural activity could

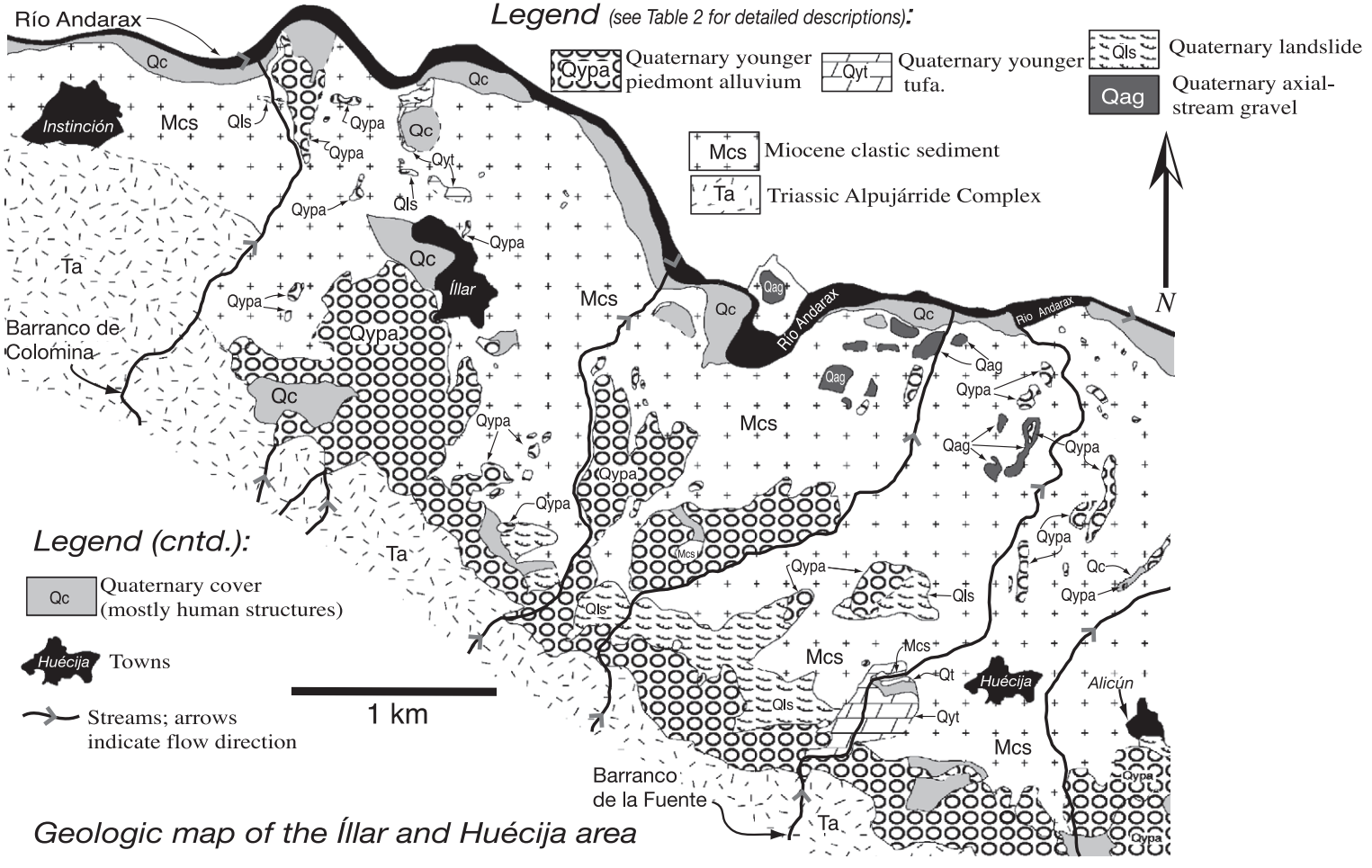

Fig. 13. Geologic map of the Sierra de Gádor piedmont near Íllar and Huécija. Notice that Qpg1 deposits are absent.

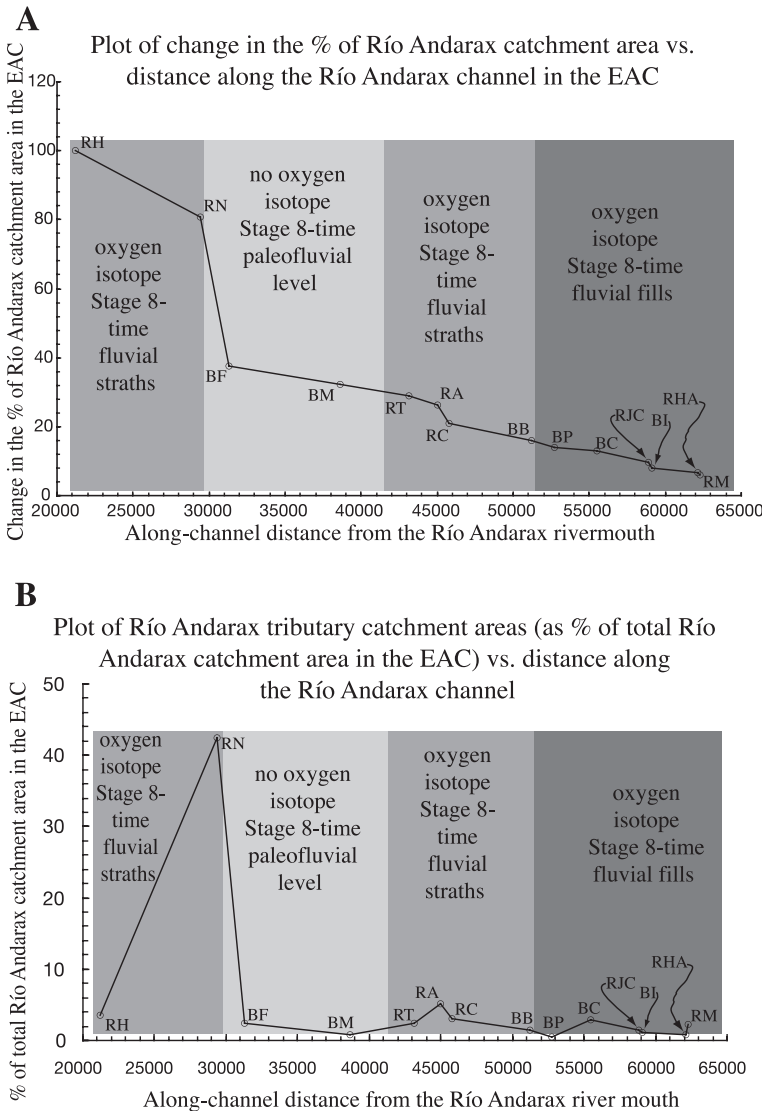

Fig. 14. Two plots showing changes in catchment area along the Río Andarax channel. The circles in the plots indicate confluences of tributaries with Río Andarax. The lines connecting the circles are extrapolations between adjacent tributaries. In both plots changes in OIS8-time relative stream power, inferred from morphostratigraphy of Río Andarax tributary-derived deposits, do not correlate with changes in the catchment area of Río Andarax. (A) The plot tracks the increase in catchment area with increasing distance downstream. There is no anomalous increase in catchment area in the Íllar and Huécija area (where no OIS8-time paleofluvial level is preserved). The largest increase in catchment area is at the Río Nacimiento-Río Andarax confluence, which is at the upstream end of a reach dominated by fluvial straths. In addition, the Río Nacimiento-Río Andarax confluence is directly north of the large strath east of the town of Alicún. (B) Plot of the contribution of major Río Andarax tributaries to the total catchment area of Río Andarax in the EAC, as a function of distance along the Andarax channel. Although the catchment area of Río Nacimiento accounts for more than 40% of the Andarax catchment in the EAC, the map pattern of OIS8-time fluvial landforms does not reflect this abrupt increase in catchment area. Tributary names, catchment areas, and figures where the tributary stream is shown: RH, Rambla de Huechar, 46 km^2, Fig. 6; RN, Río Nacimiento, 541 km^2, Fig. 6; BF, Barranco de la Fuente, 31 km^2, Fig. 13; BM, Barranco de Martín, 10 km^2, about 1 km west of the town of Instinción, Fig. 13; RT, Rambla de Tices, 40 km^2, Fig. 7; RA, Rambla de Alcora, 65 km^2, Fig. 7; RC, Río Chico, 38 km^2, Fig. 7; BB, Barranco del Bosque, 19 km^2, Fig. 8; BP, Barranco del Pilar, 7 km^2, Fig. 8; BC Barranco de Cacín, 37 km^2, Fig. 8; RCJ, Rambla de Juan de Campos, 19 km^2, Fig. 10; BI, Barranco del Infierno, 15 km^2, Fig. 10; RHA, Rambla Hoya de los Alamos, 9 km^2, Fig. 10; RM, Rambla de los Mártires, 29 km^2, Fig. 10. Catchment areas were measured on 1:25,000 scale maps using a digital planimeter.

obliterate Stage II or greater features and, thus, soils formed in Qpg2 had at most Stage I carbonate accumulation prior to cultivation. Qpg2 soils vary in color from slightly reddish gray to strongly red. Descriptions of the soil properties of a typical "gray soil" and a typical "red soil" are presented in Table 4.

4.5.1. Interpretation of Qpg2 morphostratigraphy

The map pattern of Qpg1 and Qpg2 deposits in the Laujar de Andarax area, especially at Rambla Hoya de los Alamos, indicates that the same feeder streams that deposited Qpg1 also deposited Qpg2 (Fig. 10). The widespread distribution of Qpg2 deposits indicates that they are major fills (sensu Bull, 1990; García, 2001). Therefore, when Qpg2 was deposited, critical power exceeded available power in Río Andarax and its tributaries west of Fondón (Fig. 3). This is noteworthy because after deposition of Qpg1, available power exceeded critical power in all EAC streams downstream of Rambla de Juan de Campos/east of Fondón (García, 2001; also see discussions above; Figs. 3 and 10).

The through-trenched fans (sensu Harvey, 1990) of the Vega de Laujar area provide critical insight regarding temporal changes in sediment availability in the EAC. Mapping and morphometric analysis results indicate that fan trenching was not caused by tectonism (García, 2001). Incision of feeder streams into alluvial fans in many parts of southern Spain was due solely to a late Pleistocene decrease in sediment availability (e.g., Harvey, 1984, 1987, 1990; Harvey et al., 1999a). Thus, it seems likely that the Vega de Laujar fans in the westernmost EAC were also dissected as a result of a late Pleistocene decrease in available sediment.

5. Geochronology and correlations

In this section, evidence is presented indicating that Qpg1 deposits are temporally correlative to each other and to the AdA sequences. The evidence also indicates that both AdA sequences and Qpg1 were deposited during oxygen isotope Stage 8 ("OIS8"). Additionally, the numeric age of Qpg2 is estimated on the basis of soil properties and comparison to alluvial fan sequences elsewhere in southern Spain.

5.1. Analyses of calcrete crusts and correlation of Qpg1 landforms

5.1.1. Macromorphology of Qpg1 calcretes

Qpg1 calcretes are massive, and their degree of cementation does not vary with depth. Laminar calcium carbonate is rare and is present only as centimeter-wide veins along vertical fractures. Gravel clasts in Qpg1 calcretes are mostly matrix supported, and brecciated clasts are rare but locally common. Dilation of calcrete-cemented Qpg1 deposits is evinced by their matrix-supported character, because unweathered Qpg1 gravels below calcrete horizons are mostly clast supported. Brecciated clasts also indicate strong dilation. Debris from degraded pedogenic or groundwater calcrete horizons, which is often present on mature, calcretized fan–fan surfaces in southern Spain (Alonso-Zarza et al., 1998), is present only on the Bocharalla Qpg1 complex eastern fan–fan lobe (discussed below). The macromorphological attributes outlined in this paragraph strongly suggest that Sierra de Gádor Qpg1 calcretes formed by precipitation from groundwater rather than by pedogenic processes

Table 4
Qpg2 soil properties

Pedon[a]	Munsell color (dry, wet)	Peds[b]	Dry consistence	Wet consistence	Plasticity	Texture	% Gravel
Qpg2 "grey" 1	10YR 6/3, 10YR 4/4	subangular blocky, 4–6 cm	hard to slightly hard	slightly sticky	plastic	clay loam	35
Qpg2 "grey" 2	10YR 6/3, 10YR 4/4	subangular blocky, 3–5 cm	hard to slightly hard	slightly sticky	plastic	clay loam	50
Qpg2 "red"	5YR 5/6, 2.5 YR 4/6	subangular blocky, mostly 6–8 cm, commonly >10 cm	hard to very hard	sticky to very sticky	very plastic	silty clay	35

[a] The pedogenic material described was directly on the surface of a recently plowed almond orchard. Filaments, nodules, and clast coatings of $CaCo_3$ are absent.

[b] "Peds" are soil aggregates that mantle the freshly plowed orchard. Sizes are median ped diameters.

(Wright and Tucker, 1991; Nash and Smith, 1998). This interpretation is supported by the petrographic character of the calcretes, which is discussed below (García et al., 2003).

5.1.2. Petrography of Qpg1 calcretes

In order to evaluate interpretations based on macromorphology, petrographic analyses were conducted on calcrete samples collected from each Qpg1 landform (except the Alcora Qpg1 complex). Most samples were collected within the upper 1–2 m of the Qpg1 landform tread (Table 5). The only sample collected from greater depth is sample B-2, which was collected from a fresh road cut 5.6–6.0 m below the tread of the eastern lobe of the Bocharalla fan complex (Fig. 7).

Qpg1 calcrete petrography is consistent with interpretations based on macromorphology. Microfabric features present in pedogenic calcretes in other parts of southern Spain, which include glaebules, nodules, calcified filaments and root cells, as well as alveolar septal structures (Alonso-Zarza et al., 1998; Nash and Smith, 1998), are absent from most samples (Fig. 15). Of these features, only glaebules were found, and are present in two samples (samples B-1 and B-2 from the eastern Bocharalla fan complex, discussed below; Fig. 16). Clasts in all samples typically have micrite and/or spar coatings. Some coats consist of alternating bands of micrite and spar, suggesting multiple episodes of weathering (evinced by micritization), and dissolution and reprecipitation (evinced by spar crystallization; Fig. 15). Clasts are "floating" in their matrices, are commonly angular and etched, and fractured clasts with micrite or spar infillings are common. All the characteristics of Qpg1 calcretes described in this paragraph are typical of groundwater calcretes (Wright and Tucker, 1991).

The fabrics of Qpg1 calcrete matrices are typically entirely crystalline, and consist of about half micrite or finely crystalline spar, and half spar. In some instances, the spar is present as infilling between irregular, subangular masses of micrite, and in others micrite is present as infilling between irregular, angular masses of spar crystals. Pores are commonly filled with spar, and to a lesser extent micrite and microspar (Fig. 15). These fabrics and features are similar to micromorphologic fabrics and features described by Nash and Smith (1998) in groundwater calcretes of the Tabernas Basin, which is at the east end of the Alpujarran Corridor (Fig. 2).

The Qpg1 calcrete microfabrics are very different than the microfabrics of pedogenic calcretes in the Tabernas Basin described by Nash and Smith (1998), and different than microfabrics of pedogenic calcretes elsewhere in southern Spain described by Alonso-Zarza et al. (1998). These differences, as well as the similarity of macro and micromorphologic features of Qpg1 calcretes to macro- and micromorphologic features of groundwater calcretes elsewhere in southern Spain, indicate that calcretes formed in Qpg1 are groundwater calcretes. The only Qpg1 calcrete that is not a typical groundwater calcrete is the calcrete on the eastern lobe of the Bocharalla Qpg1 complex.

5.1.3. Macromorphology and petrography of the eastern lobe of the Bocharalla Qpg1 complex

The surface of the Bocharalla Qpg1 complex eastern lobe (Fig. 9) is similar to Stage 6a fan surfaces of Alonso-Zarza et al. (1998) in that areas of laminar calcrete are at the surface, and there are also areas mantled by caliche rubble. These similarities suggest that the eastern lobe calcrete is pedogenic, but its micromorphology suggests a more complex history. In sample B-1, micritic glaebules are common and are typically arranged as masses cemented together in a spar matrix. This relationship suggests that the glaebules formed in a pedogenic environment, and were subsequently cemented and calcretized in a groundwater environment (Nash and Smith, 1998). The fabric locally consists of interlocking crystals of spar, microspar, and micrite, which also suggests groundwater calcretization (Wright and Tucker, 1991; Nash and Smith, 1998). In sample B-1, angular masses of spar crystals have well developed micritic coats, which suggests multiple episode of dissolution and weathering in a groundwater environment (Wright and Tucker, 1991; Nash and Smith, 1998).

Sample B-2 was collected from deeper below the tread of the eastern lobe than sample B-1 (Table 5) and has features notably different from those in B-1. The spar and micrite fabric is much more prevalent, and micritic glaebules are less common. The micritic glaebules are present as isolated masses surrounded

Table 5
Summary of calcrete sampling site characteristics

Sample	Landform	Sampling locality	Depth below tread	Notes
B-1	E. lobe of the Bocharalla Qpg1 complex	Distal area, 10.5 m west of the road cut at the eastern edge of the eastern-lobe tread (Fig. 7).	0 m	The sample was chiseled directly from calcrete at the surface of the lobe. The character of the surface is typical of a pedogenic calcrete-crust formed in calcareous gravel elsewhere in S. Spain (A.M. Harvey, personal communication).
B-2	E. lobe of the Bocharalla Qpg1 complex	A recent road cut at the eastern edge of the eastern lobe (Fig. 7).	5.5–6 m	This sample was chiseled directly off of the face of an excellent, fresh road cut exposure. It was collected from the bottom of the exposure.
B-3	Western lobe of the Bocharalla Qpg1 complex	South-dipping part of the western-lobe tread (Fig. 7).	0 m	Great care was taken to obtain a fresh, unweathered sample. It was collected from a microkarst "tower" whose summit is 23 cm above the adjacent "valley". The sample included the upper 5 cm of the microkarst tower.
A-1	Padules/Almócita Qpg1	~ 0.8 km SW of the town of Padules as shown in Fig. 8, on the canyon wall above Barranco del Bosque.	0.5– 0.6 m	The sample was collected from the most areally extensive, best exposed and preserved part of the Padules/Almócita Qpg1. The excellent exposure facilitated collecting a sample that is typical of the Padules/Almócita Qpg1 calcrete.
C-1	Los Llanillos de Cacín Qpg1 complex	NW corner of the Los Llanillos fan complex, at a degraded edge of the tread (Fig. 8).	1.5–2 m	Although the sample was taken from below the tread, its macromorphological character was identical to calcrete exposed on the fan treads.
F-1	Juan de Campos Qpg1 landform	Collected from a microkarst tower above a road cut 50 m west of Rambla de Juan de Campos (Fig. 10).	0 m	The sample was taken 200 m north of the downstream end of the embayed mtn. front (Fig. 10). The sample is identical to calcrete exposed in the road cut below the sampling site, but is less weathered than the road cut exposure.
Be-1	Barranco del Infierno Qpg1	E of Bco. del Infierno, SE corner of the Qpg1 exposure (Fig. 10).	0.9–1 m	Grades upward to a weathered calcrete (former tread [?]) that is buried by mine tailings. Overlies a buried Btk horizon, which has carbonate nodules (Stage II + calcic horizon).
FV-1	Qpg1 1.9 km SSW of Fuente Victoria	Stream-bank cut of Rambla Hoya de los Alamos (Figs. 10 and 12).	1.5–2 m	The sample was collected from the top of the stream-cut exposure, but it is well below the tread (Fig. 12).
FV-2	Qpg1 1.9 km SSW of Fuente Victoria	The tread in the central part of the larger Qpg1 exposure in the Rambla Hoya de los Alamos mountain-front embayment (Fig. 10).	0 m	The exposure of Qpg1 that the sample was collected from is the tread of the exposure that sample FV-1 was collected from. The sample is from the upper 10 cm of a microkarst tower.

by a micrite and spar fabric similar to that of sample B-1 (Fig. 16). This fabric is interpreted as indicating groundwater calcretization in the lower part of an actively forming pedogenic calcrete (cf. Nash and Smith, 1998).

5.1.4. Implications of calcrete development and morphology regarding landscape evolution and correlation of Qpg1 deposits

On alluvial fans, soils that have well developed calcrete horizons degrade when sediment supply is

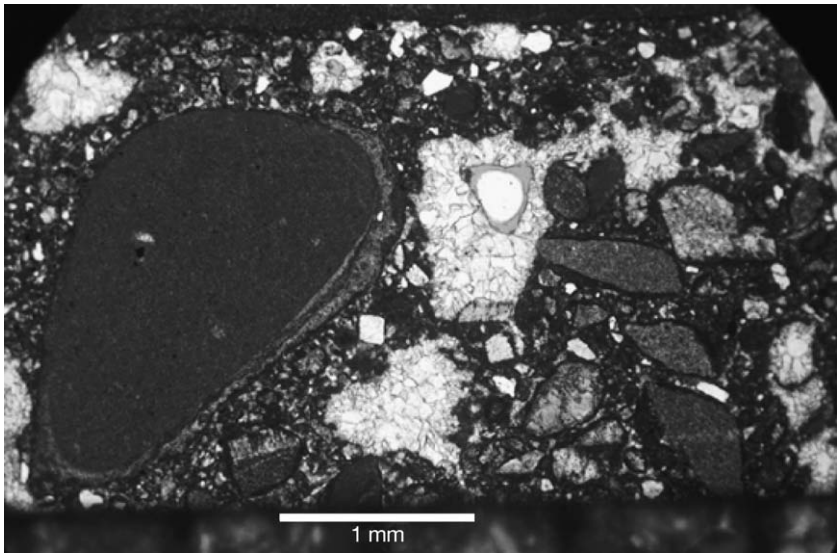

Fig. 15. Petrographic thin section of sample B-3 under plain light. The translucent, coarsely crystalline areas are pore spaces filled with spar. The gray area in the center of the photo, which engulfs an ellipsoidal white area and is within the spar-filled pore space, is a pore space stained with blue dye. Most clasts have well-developed micritic rims. For example, the alternating dark and light bands that form a thick rim on the upper right of the largest clast are spar (light bands) and micrite (dark bands).

cut off because of a decrease in permeability (Alonso-Zarza et al., 1998). Once a calcrete layer forms within the pedon of an ''abandoned'' fan surface, friable soil material above the calcrete is quickly eroded and the calcrete is exhumed (Alonso-Zarza et al., 1998). Additional fan-surface degradation occurs because surface runoff is enhanced on the impermeable calcrete that comprises the fan surface (Alonso-Zarza et al., 1998).

Set within the framework established by Alonso-Zarza et al. (1998), the micromorphology of the Bocharalla-eastern-lobe calcrete provides important clues regarding calcrete and landscape development in the EAC. The hybrid, pedogenic/groundwater character of the eastern lobe calcrete indicates pedogenic calcretization occurring above, and at the same time, as groundwater calcretization (Nash and Smith, 1998). Throughout the EAC, Qpg1 sedimentology and landscape settings are similar; therefore, it is likely that calcretization processes in Qpg1 landforms throughout the EAC were also similar. It is also likely that throughout the EAC pedogenic calcretes were present above Qpg1 groundwater calcretes. The pedogenic calcretes were stripped when feeder streams incised below Qpg1 surfaces and sediment supply was cut off (cf. Alonso-Zarza et al., 1998; García, 2001; García et al., 2003).

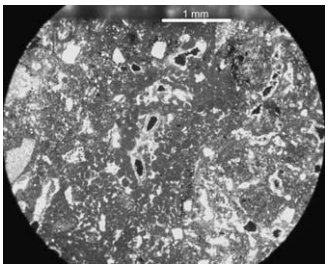

Fig. 16. Petrographic thin section of sample B-2 under plain light. A cluster of micritic glaebules form a diagonal band across the view in the photo. The band is in a matrix of micrite and spar, in the upper left and lower right of the photo.

Calcrete-landform relationships documented in the Tabernas Basin (Nash and Smith, 1998) provide additional insight regarding calcrete-landform relationships in the EAC. Two levels of relatively well preserved (compared to Qpg1 landforms in the EAC) relict piedmont surfaces underlain by alluvial gravels are present throughout the Tabernas Basin (Nash and Smith, 1998). Both relict piedmont sequences consist of a basal groundwater calcrete below a gravel bed which grades upward into a pedogenic calcrete (Nash

and Smith, 1998). Groundwater and pedogenic calcretization probably occurred simultaneously in relict piedmont sequences of the Tabernas Basin that occupy the same paleoalluvial level (Nash and Smith, 1998). This suggests that within single drainage basins in southern Spain, groundwater calcretes occupying a similar paleoalluvial level can be used for chronostratigraphic correlation in the same way that pedogenic calcrete morphology can be for chronostratigraphic correlation. EAC Qpg1 calcretes occupy the same paleoalluvial level (Garcia, 2001), and as indicated by the petrography of the Bocharalla eastern lobe calcrete, probably formed below pedogenic calcretes. Thus, it is likely that the exhumed groundwater calcretes of the EAC Qpg1 are chronostratigraphically equivalent, and reflect a similar, relatively advanced (compared to the Tabernas Basin relict piedmont sequences) state of landform development wherein pedogenic calcretes and uncalcretized gravels have been stripped.

The Bocharalla Qpg1 complex eastern lobe calcrete is less degraded than other Qpg1 calcretes in that it is mantled by caliche rubble, and the microfabrics of calcretes on the eastern lobe include features associated with pedogenic calcrete. The relatively well-preserved character of the eastern lobe calcrete is in part due to its closeness to the Sierra de Gádor mountain front, which insures an ample supply of sediment (García et al., 2003). The relatively small catchment area of streams that feed the eastern lobe precluded their incision below its calcretized surface and, therefore, the calcretes are stabilized by ongoing sediment deposition (García et al., 2003).

5.2. Correlation of Qpg1 to AdA sequences

In this section, Qpg1 deposits are correlated to each other and to AdA sequences on the basis of landscape position and altitude. Chronostratigraphic correlation of Qpg1 and AdA sequences is also established by evaluating their depositional history in the context of regional models of climatically driven cycles of fluvial aggradation and degradation. The reasons for establishing these correlations is to evaluate the pattern of paleostream power in the Río Andarax network during Qpg1 and AdA sequence deposition, and to establish the numeric age of Qpg1 deposits.

The AdA sequences and Qpg1 deposits occupy the same landscape position. Qpg1 and AdA tufa landforms are locally buried at mountain fronts, but otherwise they are the highest constructional geomorphic surfaces in the EAC (Fig. 17). Although they are not physically continuous, the geomorphic surfaces of the AdA sequence landforms and the Qpg1 landforms are at the same paleoalluvial level, and comprise a former valley floor and/or a piedmont flanking a valley floor (Fig. 4; García et al., 2003). These landscape relationships strongly suggests that AdA sequences and Qpg1 are temporally correlative.

The height of AdA sequence and Qpg1 bases above the present-day channel of the EAC axial stream (Río Andarax) is not consistent (Fig. 18; Table 2). However, AdA sequences and Qpg1 deposits originate from tributaries and dip towards the Río Andarax, and their distal extremities are eroded by varying amounts. As a result, the bases of the AdA sequences and Qpg1 deposits nearest to the modern Río Andarax channel do not precisely reflect the former altitude of Río Andarax. The critical data suggesting that AdA sequences and Qpg1 deposits comprise a common paleoalluvial level are the consistently higher altitude of Qpg1/AdA sequence bases as distance from the mouth of Río Andarax increases (Fig. 18; Table 2).

5.3. Numeric ages of AdA sequences and Qpg1

EAC geochronology is based on Th/U series analyses of tufa samples collected from AdA sequences, which indicate that they were deposited during OIS8 (Table 6; García, 2001; García et al., 2003). The numeric age of AdA sequences is also based on models of climatically induced cycles of alluvial aggradation and degradation in the EAC (García, 2001; García et al., 2003) and southern Spain (e.g., Harvey, 1990). Fluvial systems throughout southern Spain aggraded during glacial periods, and incised during interglacial periods (e.g., Harvey, 1990; Harvey et al., 1999a). In southern Spain during glacial times, the combination of more potent storms (than during interglacials) impacting sparsely vegetated hillslopes, high sediment availability, and relatively low overall precipitation, caused increased sediment delivery to streams and aggradation (Harvey, 1984, 1990; Harvey et al., 1999a). Fluvial incision prevailed during inter-

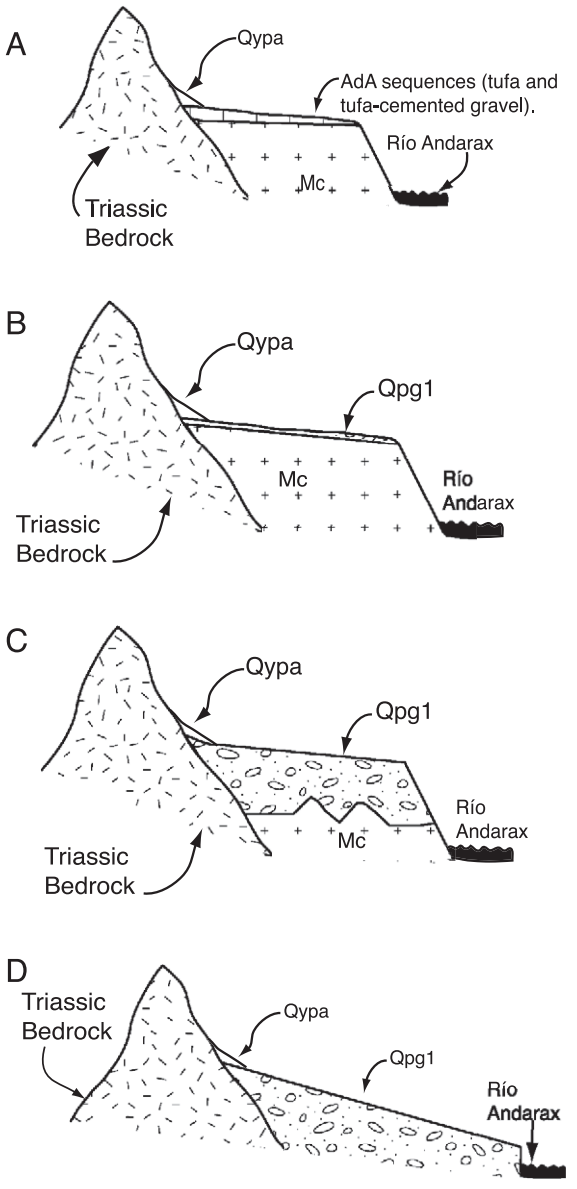

Fig. 17. Cartoon of the geomorphic position of Qpg1 landforms east of Fondón (west of Fondón Qpg1 is present only as partly exposed fan remnants) and of the AdA sequences. Surfaces underlain by Qpg1 and AdA sequences intersect the mountain front at a higher level than any other geomorphic surfaces. The cartoons represent the geology of the following areas: A, Alhama de Almería environs (Fig. 6); B, Bocharalla/Alcora and Almócita/Padules (Figs. 7 and 8); C, Los Llanillos de Cacín (Fig. 8); D, Rambla de Juan de Campos/Barranco del Infierno Qpg1 (Fig. 10).

glacial times because of increased vegetative cover (Pons and Reille, 1988), slower rates of weathering and sediment production, and a net decrease in sediment delivery to streams relative to glacial times (Harvey, 1984, 1990; Harvey et al., 1999a).

Many studies showed that in southern Spain, as a consequence of abundant sediment supply in stream catchments, the middle Pleistocene (middle Pleistocene: 780–200 ky; Berggren et al., 1995) was a 'maximum' time of fluvial aggradation (e.g., Harvey, 1990). The depositional age of AdA sequences, then, corresponds to a glacial period (OIS8) during the Middle Pleistocene fluvial-aggradation maximum in southern Spain. Therefore, the landscape relationship of AdA sequences to Qpg1 deposits, considered in the context of models of climatically driven cycles of fluvial aggradation and degradation in southern Spain, as well as in the context of the Th/U series age of the AdA sequences, indicate that both were deposited during OIS8 (García, 2001). This conclusion is consistent with the numeric age of tufa overlain by Qpg1 at the Bocharalla Qpg1 complex, which is >350 ka (sample BFC-1; Table 6).

5.4. Inferred age of Qpg2

The numeric age of Qpg2 is estimated by comparison of the Vega de Laujar alluvial fan sequences to alluvial fan sequences elsewhere in southern Spain. The age of Qpg2 is also estimated by comparing soil properties of pedons formed in Qpg2 to soil properties of pedons formed in dated sediments elsewhere in southern Spain. Estimating the ages of Qpg2 is necessary to evaluate the distribution of paleostream power in the EAC during the latest Pleistocene.

Alluvial-fan sequences at the Vega de Laujar are similar to alluvial-fan sequences in the western part of the Cabo de Gata area of southern Spain ("western fans" of Harvey et al., 1999a; Fig. 2). The Cabo de Gata western fans contain extensive "Qf3" lobes, which consist of latest glacial-age sediments (70–10 ka; Harvey et al., 1999a). These are inset into the oldest fan lobes of the Cabo de Gata western fans ("Qf1"). Qf1 lobes in the Cabo de Gata area are of pre-Tyrrhenian II age (oxygen isotope Stage 5; Harvey et al., 1999a), have Stages III–IV calcic and petrocalcic soils, and on the western fans are present

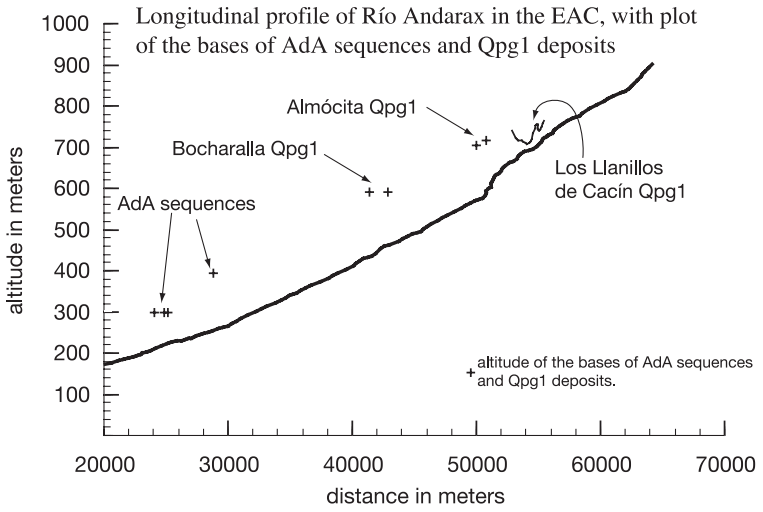

Fig. 18. Plot showing altitude of the bases of AdA sequences and Qpg1 deposits relative to each other and to the longitudinal profile of Río Andarax. Numerous data points allow plotting the base of the Los Llanillos de Cacín Qpg1 as a line. Altitude data are summarized in Table 3.

only as small exposures near the fan apex (Harvey et al., 1999a). These characteristics are similar to the Vega de Laujar fans, where Qpg2-dominated fan surfaces are inset into relatively small calcretized Qpg1 fan deposits that are present only near fan apexes (Fig. 10). Thus, the morphostratigraphic relationship of Qpg1 to Qpg2 fan lobes in the Fuente Victoria fan is similar to relationships of Qf1 to Qf3 in the Cabo de Gata western fans (Fig. 10). This suggests that the Vega de Laujar Qpg2 deposits may be chronostratigraphically equivalent to the Cabo de Gata Qf3 deposits of Harvey et al. (1999a), and were deposited during the last glacial period (oxygen isotope Stage 2 [OIS2]).

This contention is supported by evaluation of Qpg2 soil properties, which strongly suggests that Qpg2 was deposited during or after OIS2. In southern Spain, fully cemented pedogenic calcretes (Stages IV–VI K horizons of Machette, 1985) typically form in as little as 250 ka (Alonso-Zarza et al., 1998). The clast composition of Qpg2 gravels is similar to the clast composition of the "Terrace C" fluvial gravels in the Sorbas Basin of southern Spain (Fig. 2), whose age is between 80 and 110 ka (Harvey et al., 1995; Kelly et al., 2000). The Sorbas Basin Terrace C soils are characterized by Bk horizons with Stage II carbonate accumulation (Harvey et al., 1995). Other Sorbas basin soils formed in gravelly alluvium whose esti-

Table 6
Th/U analyses of tufa-fossilized plant stems collected in the eastern EAC

Sample, altitude of sampling site, map unit	U (ppm)	$^{234}U/^{238}U$ activity ratio	$^{230}Th/^{232}Th$ activity ratio	$^{230}Th/^{234}U$ activity ratio	Age (ky)
T-7, 540 m, Qtd (1)	0.72 ± 0.02	1.11 ± 0.03	70.5 ± 10.1	0.95 ± 0.03	276 ± 40
T-12, 385 m, Qlst (1)[a]	1.81 ± 0.04	1.01 ± 0.02	168 ± 25	0.97 ± 0.03	354 ± 76
T-13a, 325 m, Qt (1)	1.30 ± 0.03	1.04 ± 0.03	101 ± 16	0.91 ± 0.03	248 ± 29
T-15, 310 m, Qtd (1)	0.89 ± 0.02	1.04 ± 0.02	90.9 ± 12.2	0.94 ± 0.02	282 ± 34
BFC-1, 585 m, Mcs (2)[b]	–	–	–	–	>350

(1) Uncertainties are standard deviations derived from counting statistics. Samples collected near Alhama de Almería (Fig. 6) and analyzed at the University of Southern California Geochemistry Laboratory, USA.
(2) Sample BFC-1 was collected at the Bocharalla Qpg1 Complex (Fig. 7) and analyzed at the Laboratorio de Radiochronología del Instituto Jaume Almera, CSIC, Barcelona, Spain.
[a] Landslide deposit in buttress unconformable contact with Qt.
[b] Unconformably overlain by Qpg1.

mated age range is 50–10 ky have Bk horizons with Stage I carbonate accumulation (Harvey et al., 1995). Qpg2 soils had at most Stage I calcic horizons prior to cultivation, therefore, they must be markedly younger than the 80–110 ka Terrace C soils of the Sorbas Basin and may be equivalent to the 50–10 ka. Soils of the Sorbas basin studied by Harvey et al. (1995).

Alternatively, given the weakly developed carbonate features in Qpg2 soils, Qpg2 may have been deposited during the early or middle part of the Holocene. Deposition of up to 20 m of alluvium occurred in the Guadalentin Valley of southern Spain (Murcia) between 10 and 3.5 ka (Calmel-Avila, 2000). Therefore, aggradation during interglacials in southern Spain cannot be ruled out and it is possible that Qpg2 was deposited after OIS2. Deposition of Qpg2 was followed by fan through trenching of Qf2 fan surfaces and deposition of Qpg3 (Fig. 10 and Table 1), which suggests that Qpg2 deposition was complete some time before the latest Holocene.

Based on Qpg2 soil properties, on the present understanding of soil forming processes and rates in southern Spain, and the morphostratigraphic similarity of the Vega de Laujar fans to the Cabo de Gata western fans, it is concluded that Qpg2 was probably deposited during OIS2, but may have been deposited as recently as 3.5 ky.

6. Middle to late Pleistocene patterns of available stream power in the Río Andarax fluvial network

6.1. Summary of conclusions regarding fluvial processes in the eastern Alpujarran Corridor

AdA sequences and Qpg1 were deposited during oxygen isotope Stage 8 and constitute the most areally extensive paleoalluvial level in the EAC. Prior to, during, and after OIS8, the EAC was affected by tectonically induced, regional base-level fall (García, 2001; García et al., 2003). Additionally, because of the shallow continental shelf at the mouth of Río Andarax, the role of Quaternary eustatic fluctuation is negligible in the mid Quaternary to Recent evolution of the EAC fluvial system (García, 2001; outlined in detail in García et al., 2003).

In the EAC, episodes of major fluvial aggradation (sensu Bull, 1990) occurred as a consequence of climatic events, which caused increased sediment delivery to streams (García, 2001; García et al., 2003; cf. Bull, 1979, 1990; Harvey, 1990). The climatic event that led to deposition of Qpg1 and the AdA sequences was the oxygen isotope Stage 8 (“OIS8”) glacial period. The climatic event that led to deposition of Qpg2 alluvial fan lobes in the Laujar de Andarax environs was probably oxygen isotope Stage 2 (“OIS2”), but Qpg2 may have been deposited in the Holocene (deposition complete by 3.5 ka).

6.2. Relative stream power during OIS8

The AdA sequences are relatively thin and overlie straths cut by Río Andarax tributaries. This observation indicates that Río Andarax tributaries downstream of Alicún (Fig. 3) were at the threshold of critical stream power during OIS8 (Bull, 1979, 1990).

There is no OIS8-time paleoalluvial level between Alicún and Rágol (Fig. 3). As discussed in detail above, the absence of the OIS8-time paleoalluvial level indicates that during OIS8, available power exceeded critical power in this part of the EAC. Therefore, between the towns of Alicún and Rágol (Fig. 3), available power exceeded critical power during OIS8.

Fluvial straths overlain by relatively thin Qpg1 deposits indicate that during OIS8, Andarax-tributary streams between Rágol and Almócita (Fig. 3) were at the threshold of critical stream power (Bull, 1979). Upstream of Almócita, along the remainder of Río Andarax’s channel in the EAC, Qpg1 consists of thick alluvial fills that overlie irregular unconformities, or whose bases are below present-day channels. This conclusion indicates that critical power exceeded available power during OIS8 in Río Andarax tributaries upstream of Almócita (Fig. 3; e.g., Bull, 1979; 1990).

6.3. Pattern of available stream power during oxygen isotope Stage 8

If all other factors are equal, climatically induced increases in critical power lead to similar stream response within a drainage basin (e.g., Bull, 1990; Personius, 1995). Therefore, the OIS8-time distribu-

tion of *relative stream power* in the EAC reflects the OIS8-time distribution of *available stream power* in the EAC. The pattern of OIS8-time available power in the EAC is incision-wave like (Fig. 19).

Incision rates in numeric simulation are controlled by temporal variations in available stream power along channels in the modeled fluvial network (Anderson, 1994; Rosenbloom and Anderson, 1994; Safran, 1998). Similarly, the pattern of available power in the EAC during OIS8 reflects the position of an incision wave in the EAC during a 58-ka time interval. The crest of the incision wave during OIS8 was between Alicún and Rágol, which is the only area in the EAC where available stream power exceeded critical stream power during OIS8 (Fig. 19). Stream power and critical power were equal in the EAC downstream of Alicún, and between Rágol and Almócita. These areas represent, respectively, the upstream and downstream limbs of the incision wave. The area upstream of Almócita, where thick fills were deposited during OIS8, had not been affected by the incision wave prior to or during OIS8.

6.4. Relative stream power distribution during Qpg2 time

The distribution of relative stream power in the EAC when Qpg2 was deposited was markedly different than it was during OIS8. Sediments deposited during Qpg2 time are restricted to the upper reaches of Río Andarax in the EAC. Little or no alluvium other than Qpg1 and active channel gravel is present in Andarax tributaries downstream of and including Rambla de Juan de

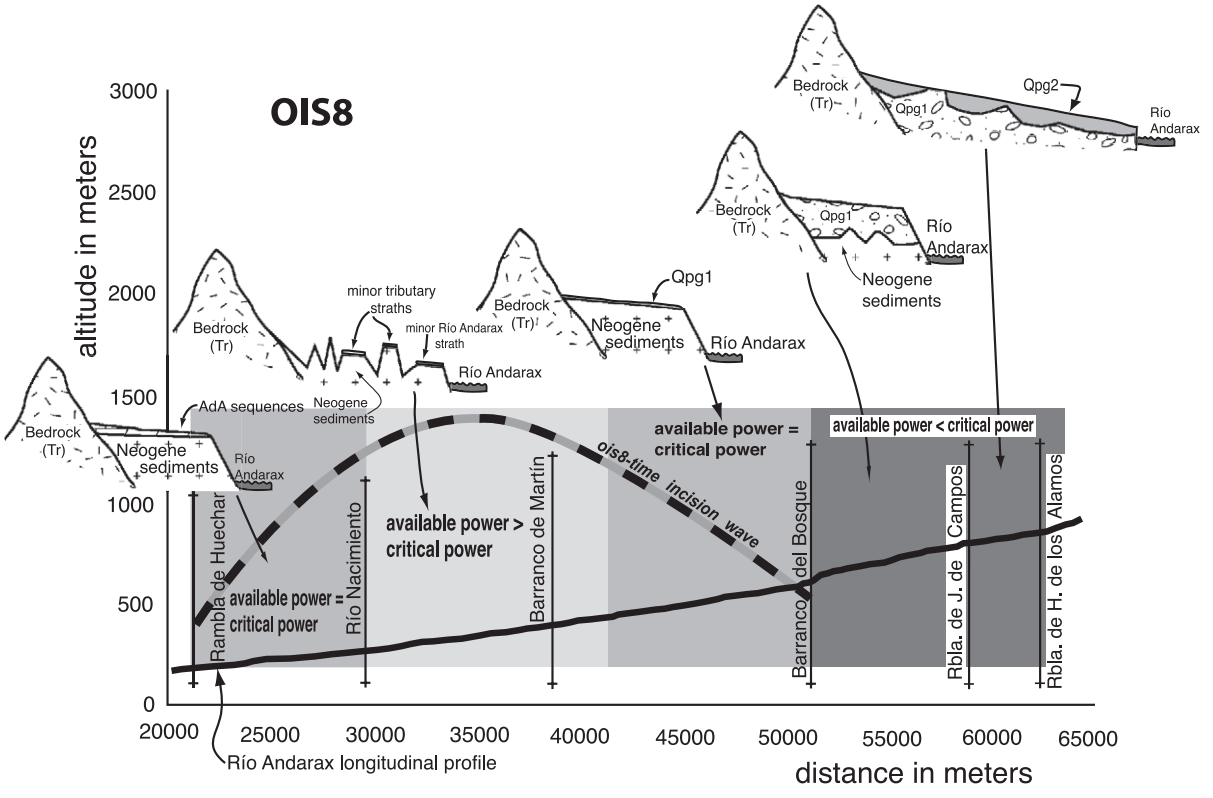

Fig. 19. Cartoon and summary of EAC fluvial stratigraphy, with interpretations of relative stream power based on landform morphostratigraphy. The incision wave as recorded in OIS8-time fluvial sediments and landforms is shown schematically (its position relative to the *y* axis of the longitudinal-profile plot is arbitrary). The vertical black lines indicate the distance from the Río Andarax river mouth to where major tributaries join Río Andarax.

Campos (Figs. 3 and 10). This indicates that during Qpg2 time, available power exceeded critical power in Río Andarax tributaries downstream of and including Rambla de Juan de Campos. Río Andarax and Río Andarax tributaries upstream of Rambla de Juan de Campos deposited Qpg2 alluvial fan lobes where they flow into the EAC from Sierra Nevada or Sierra de Gádor. This indicates that critical power exceeded available power in the EAC upstream of Rambla de Juan de Campos during Qpg2 time.

6.5. Pattern of available stream power during Qpg2 time

Climatically induced increases in critical power result in similar stream response within a drainage basin when all other factors are equal (e.g., Bull, 1990; Personius, 1995). It is, therefore, likely that the Qpg2-time distribution of relative stream power in the EAC reflects the Qpg2-time distribution of available stream power in the EAC. The downstream-to-upstream change in available stream power in the Río Andarax stream network during Qpg2 time was abrupt and threshold like (Fig. 20). For example, the confluence of Río Andarax and Rambla Hoya de los Alamos is only 3.2 km upstream of the confluence of Río Andarax and Rambla de Juan de Campos (Fig. 10). Rambla Hoya de los Alamos deposited a Qpg2 alluvial fan lobe, but Rambla de Juan de Campos was incising vertically during Qpg2 time. The pattern suggests that as soon as the upstream-migrating incision "wave" affected Rambla de Juan de Campos, available power exceeded critical power, even during the climatic events (OIS2 or OIS1) that caused fluvial aggradation

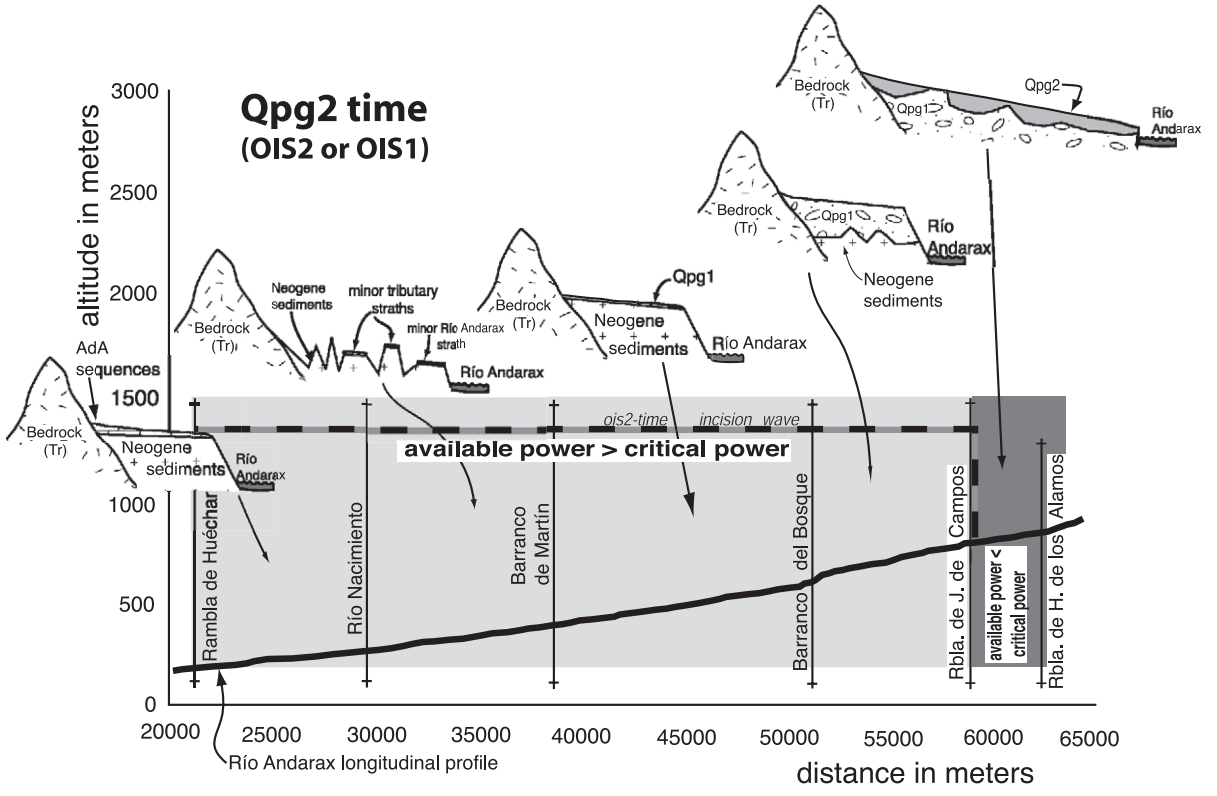

Fig. 20. Cartoon and summary of EAC fluvial stratigraphy, with interpretations of relative stream power based on landform morphostratigraphy. The incision wave as recorded in Qpg2-time fluvial sediments and landforms is shown schematically (its position relative to the *y* axis of the longitudinal-profile plot is arbitrary). The vertical black lines indicate the distance from the Río Andarax river mouth to where major tributaries join Río Andarax.

farther upstream and elsewhere in southern Spain (cf. Harvey et al., 1999a; Calmel-Avila, 2000).

7. Discussion

7.1. Rates of incision-wave propagation

Locating the position of the EAC incision wave during OIS8 and Qpg2 time allows calculating the rate at which it propagated through the Río Andarax network. For this discussion, it is assumed that Qpg1 deposition occurred during OIS8 and Qpg2 deposition occurred during OIS2 or OIS1 (complete by 3.5 ka). Thus, a range of possible rates is calculated. The upstream end of the incision wave had reached Barranco del Bosque by OIS8, and it had reached Rambla de Juan de Campos by Qpg2 time (Figs. 3, 19, and 20). Therefore, the incision wave moved 7.7 km upstream along the Río Andarax channel between OIS8 and Qpg2 time. The difference in years between the beginning of OIS8 (303 ka; Imbrie et al., 1984) and 3.5 ka is 299.5 ka, which yields a minimum rate of 26 m/ka. The difference in years from the end of OIS8 (245 ka; Imbrie et al., 1984) to the beginning of OIS2 (21.4 ka; Imbrie et al., 1984) is 223.6 ka, which yields a maximum rate of 34 m/ka.

7.2. Climatic controls on incision wave propagation

A premise of the incision wave hypothesis is that a given reach of a stream is not affected by an upstream-propagating incision wave until the adjacent downstream reach incises vertically (Safran, 1998). It follows that any process slowing vertical incision will slow incision-wave propagation rate. Strath formation requires lateral stream erosion, which happens when a stream is not incising vertically (Bull, 1979, 1990; Pazzaglia and Brandon, 2001). Straths overlain by Qpg1 gravels indicate that Río Andarax tributaries were eroding laterally rather than vertically during OIS8. Vertical incision and propagation of the incision wave through Río Andarax tributaries must have ceased during OIS8. Therefore, the OIS8 climatic event probably prevented migration of the incision wave into Río Andarax tributaries and side valleys. This conclusion indicates that extrinsic factors like climatic fluctuations may control the rate at which an incision wave propagates through a fluvial system.

7.3. Sedimentologic controls on incision wave propagation

The dramatically different patterns of relative stream power during OIS8 and Qpg2 time provide insight regarding how sediment availability affected incision-wave manifestation in the EAC. As discussed above, through-trenching of the Vega de Laujar fans is due to a decrease in sediment availability during late Pleistocene (approximately 100 ka to present; cf. Harvey, 1984, 1987, 1990; Harvey et al., 1999a). During Qpg2 time, when there was little sediment in drainage catchments, available stream power exceeded critical stream power in Andarax tributaries that were very recently affected by the incision wave (i.e., streams in the upstream limb like Rambla de Juan de Campos). The streams in the upstream limb were incising vertically because there was insufficient sediment to raise critical power and stop vertical incision. Sediment supplies had diminished in the EAC by the late Pleistocene, and as a result, the OIS2 climatic event was ineffectual at stopping vertical incision and slowing propagation of the incision wave. Therefore, averaged over time scales at which global climate fluctuated, once sediment supply from drainage catchments was depleted in the late Pleistocene/Holocene, incision-wave propagation rate in the EAC increased.

If Qpg2 is, in fact, an OIS2-time deposit, then it is conceivable that greater aggradation during OIS8 than during OIS2 occurred because of differences in the intensity of the OIS2 and OIS8 climatic perturbations (Bull, 1990). However, the $\delta^{18}O$ content of sea water was slightly greater during OIS2 than during OIS8 (Williams et al., 1988), indicating that OIS2 was colder than OIS8, and/or that glaciation was more extensive during OIS2 than OIS8. Therefore differences in stream response due strictly to climatic factors should have caused greater fluvial aggradation in OIS2 than in OIS8 (Bull, 1990).

8. Conclusions

The incision wave hypothesis simply and comprehensively accounts for the distribution and contrasting

morphostratigraphy of EAC alluvial sediments. Compelling arguments have been made questioning the applicability of the stream power equation to modeling large river systems (Sklar and Dietrich, 1998; Stock and Montgomery, 1999; Wohl and Merritt, 2001; Roe et al., 2002). If the interpretations of EAC alluvial stratigraphy made in this paper are correct, then incision waves like those predicted by models based on the stream power equation (Anderson, 1994; Rosenbloom and Anderson, 1994; Safran, 1998) can, in at least one instance, be recognized in the geologic record.

The results of this study provide insight regarding how incision wave manifestation is affected by factors extrinsic and intrinsic to the fluvial system. In the conceptual model proposed in this paper, strath genesis resulting from climatic change can temporarily halt upstream propagation of an incision wave. However, when available sediment is scarce in drainage catchments, incision waves move upstream more rapidly than when available sediment is abundant because climatic fluctuations do not stop vertical stream incision in the upstream and downstream limbs of the incision wave. These two results indicate the rate at which an incision wave translates upstream can be controlled by an interaction of intrinsic and extrinsic factors, including climatic fluctuation and sediment supply in drainage catchments.

Acknowledgements

This paper benefited greatly from reviews and suggestions made by Drs. F. Gutierrez, A.M. Harvey, P.G. Silva, E.E. Wohl, and an anonymous reviewer. Dr. M. Stokes read an early version of this manuscript and his comments greatly improved this paper. This paper is in part based on A.F. García's PhD Thesis. The ideas for this paper benefited greatly from discussion with and review of García's thesis by Drs. T.A. Atwater, T. Dunne, and A.G. Sylvester.

Special thanks from the first author to Dr. R. Saenz, Dr. P. Bailey, Dr. Daniel Lewis, and most of all to Jill García. Without their encouragement and support this paper would not have been written. Special thanks to Dr. D. Harden for years of mentorship, support, and for providing a digital planimeter.

The first author would like to thank the following people for generous support and/or assistance while conducting field work: the Valdivia López family, Dr. Alice Alldredge and James M. King, Enrique Pérez Ibarra (a friend of the first author's), Petra, Dr. A. Azor, Dr. R. El Hamdouni, Dr. C. Irigaray Fernández, Dr. K. Kleverlaan, and especially Drs. A.E. Mather and M. Stokes. Enrique Pérez Ibarra located tufa sample T-12 and directed the first author to critical tufa sampling sites. Dr. A.M. Harvey provided critical suggestions regarding calcrete analyses. Thanks to Dr. M. Sommers for assistance with calcrete petrography.

This research was funded by the following organizations and grants: Vicerrectorado de investigación y relaciones internacionales, Facultad de Ciencias, University of Granada, Spain; Geological Society of America Research Grant; Sigma Xi Grant-in-aid of Research; University of California, Santa Barbara (UCSB) Academic Senate; UCSB Department of Geological Sciences "Block Grants".

References

Alonso-Zarza, A.M., Silva, P.G., Goy, J.L., Zazo, C., 1998. Fan-surface dynamics and biogenic calcrete development. Interactions during ultimate phases of fan evolution in the semiarid SE Spain (Murcia). Geomorphology 24, 147–167.

Anderson, R.S., 1994. Evolution of the Santa Cruz Mountains, California, through tectonic growth and decay. Journal of Geophysical Research 99 (B10), 20161–20179.

Bagnold, R.A., 1973. The nature of saltation and of bed load transport in water. Proceedings of the Royal Society of London 332, 473–504.

Berggren, W.A., Kent, D.V., Swisher III, C.C., Aubry, M.P., 1995. A revised Cenozoic geochronology and chronostratigraphy. In: Berggren, W.A., Kent, D.V., Aubry, M.P. (Eds.), Geochronology, Time Scales and Global Stratigraphic Correlation, vol. 54. Society of Economic Paleontologists and Mineralogists Special Publication, Tulsa, pp. 129–212.

Bull, W.B., 1979. Threshold of critical power in streams. Geological Society of America Bulletin 90, 453–464.

Bull, W.B., 1990. Stream-terrace genesis: implications for soil development. Geomorphology 3, 351–367.

Calmel-Avila, M., 2000. Etude des paleoenvironnements holocenes dans le bassin du Bas-Guadalentin (Region de Murcie, Espagne). Geomorphologie, 147–159.

Galindo-Zaldívar, J., Jabaloy, A., González-Lodeiro, F., Aldaya, F., 1997. Crustal Structure of the central Betic Cordillera (SE Spain). Tectonics 16, 18–37.

García, A.F., 2001. Quaternary stream incision and topographic development in the eastern Alpujarran Corridor, Betic Cordil-

lera, southern Spain (Almería). PhD thesis, The University of California, Santa Barbara. 214 pp.

García, A.F., Zhu, Z., Ku, T.L., Sanz de Galdeano, C., Chadwick, O.A., Chacón Montero, J., 2003. Tectonically driven landscape development within the eastern Alpujarran Corridor, Betic Cordillera, SE Spain (Almería). Geomorphology 50, 83–110.

Harvey, A.M., 1984. Aggradation and dissection sequences on Spanish alluvial fans: influence on morphological development. Catena 11, 289–304.

Harvey, A.M., 1987. Alluvial fan dissection: relationship between morphology and sedimentation. In: Frostick, L., Reid, I. (Eds.), Desert Sediments: Ancient and Modern. Geological Society of London, London, pp. 87–103.

Harvey, A.M., 1990. Factors influencing Quaternary alluvial fan development in southeast Spain. In: Rachocki, A.H., Church, M. (Eds.), Alluvial Fans: A Field Approach. Wiley, Chichester, pp. 247–269.

Harvey, A.M., Wells, S.G., 1987. Response of Quaternary fluvial systems to differential epeirogenic uplift: Aguas and Feos river systems, southeast Spain. Geology 15, 689–693.

Harvey, A.M., Miller, S.Y., Wells, S.G., 1995. Quaternary soil and river terrace sequences in the Aguas/Feos river systems, southeast Spain. In: Lewin, J., Macklin, M.G., Woodward, J.C. (Eds.), Mediterranean Quaternary River Environments. Balkema, Rotterdam, pp. 263–281.

Harvey, A.M., Silva, P.G., Mather, A.E., Goy, J.L., Stokes, M., Zazo, C., 1999a. The impact of Quaternary sea-level and climate change on coastal alluvial fans in the Cabo de Gata ranges, southeast Spain. Geomorphology 28, 1–22.

Harvey, A.M., Wigand, P.E., Wells, S.G., 1999b. Response of alluvial fan systems to the late Pleistocene to Holocene transition: contrasts between the margins of pluvial Lakes Lahontan and Mojave, Nevada and California, USA. Catena 36, 255–281.

Howard, A.D., 1994. A detachment-limited model of drainage basin evolution. Water Resources Research 30, 2261–2285.

Howard, A.D., Kerby, G., 1983. Channel changes in badlands. Geological Society of America Bulletin 94, 739–752.

Imbrie, J., Hays, J.D., Martinson, D.G., McIntyre, A., Mix, A.C., Morley, J.J., Pisias, N.G., Prell, W.L., Shackleton, N.J., 1984. The orbital theory of Pleistocene climate: support from a revised chronology of the marine δ^{18}O record. In: Berger, A., Imbrie, J., Hays, J., Kukla, G., Saltzman, B. (Eds.), Milankovitch and Climate: Part 1. D. Reidel Publishing, Dordrecht/Boston/Lancaster, pp. 269–305.

Kelly, M., Black, S., Rowan, J.S., 2000. A calcrete-based U/Th chronology for landform evolution in the Sorbas basin, southeast Spain. Quaternary Science Reviews 19, 995–1010.

Ku, T.L., 2000. Uranium-series methods. In: Noller, J.M., Sowers, J.S., Lettis, W.R. (Eds.), Quaternary Geochronology: Methods and Applications. American Geophysical Union, Washington, DC, pp. 101–114.

Ku, T.L., Ivanovich, M., Luo, S., 1990. U-Series dating of last interglacial high stands: Barbados revisited. Quaternary Research 33, 129–147.

Machette, M.N., 1985. Calcic soils of the southwestern United States. In: Weide, D.L. (Ed.), Soils and Quaternary Geology of the Southwestern United States. Geological Society of America Special Paper, vol. 203, pp. 1–21.

Mather, A.E., Harvey, A.M., 1995. Controls on drainage evolution in the Sorbas Basin, southeast Spain. In: Lewin, J., Macklin, M.G., Woodward, J.C. (Eds.), Mediterranean Quaternary River Environments. Balkema, Rotterdam, pp. 65–76.

Mather, A.E., Stokes, M., Griffiths, J.S., 2002. Quaternary landscape evolution: a framework for understanding contemporary erosion, southeast Spain. Land Degradation and Development 13, 89–109.

Merritts, D.J., Vincent, K.R., Wohl, E.E., 1994. Long river profiles, tectonism, and eustasy: a guide to interpreting fluvial terraces. Journal of Geophysical Research 99 (B7), 14031–14050.

Nash, D.J., Smith, R.F., 1998. Multiple calcrete profiles in the Tabernas Basin, southeast Spain: their origins and geomorphic implications. Earth Surface Processes and Landforms 23, 1009–1029.

Pascual Molina, A.M., 1997. La Cuenca Neogena de Tabernas (Cordilleras Beticas). PhD thesis, The University of Granada, Granada, Spain. 285 pp.

Pazzaglia, F.J., Brandon, M.T., 2001. A fluvial record of long-term steady-state uplift and erosion across the Cascadia forearc high, western Washington State. American Journal of Science 301, 385–481.

Pazzaglia, F.J., Gardner, T.W., Merritts, D.J., 1998. Bedrock fluvial incision and longitudinal profile development over geologic time scales determined by fluvial terraces. In: Tinkler, K.J., Wohl, E.E. (Eds.), Rivers Over Rock: Fluvial Processes in Bedrock Channels. American Geophysical Union, Washington, DC, pp. 207–235.

Personius, S.F., 1995. Late quaternary stream incision and uplift in the forearc of the Cascadia subduction zone, western Oregon. Journal of Geophysical Research 100 (B10), 20193–20210.

Pons, A., Reille, M., 1988. The Holocene and Upper Pleistocene pollen record from Padul (Granada Spain). Palaeogeography, Palaeoclimatology, Palaeocology 66, 243–263.

Roe, G.H., Montgomery, D.R., Hallet, B., 2002. Effects of orographic precipitation variations on the concavity of steady-state river profiles. Geology 30, 143–146.

Rosenbloom, N.A., Anderson, R.S., 1994. Hillslope and channel evolution in a marine terraced landscape, Santa Cruz, California. Journal of Geophysical Research 99 (B7), 14013–14029.

Safran, E.B., 1998. Channel network incision and patterns of mountain geomorphology. PhD thesis, The University of California, Santa Barbara. 325 pp.

Sanz de Galdeano, C., 1996. The E-W segments of the contact between the External and Internal Zones of the Betic and Rif Cordilleras and the E–W Corridors of the Internal Zone (a combined explanation). Estudios Geologicos 52, 123–136.

Sanz de Galdeano, C., 1997. La Zona Interna Bético-Rifeña. Universidad de Granada, Granada, Spain. 316 pp.

Sanz de Galdeano, C., López Garrido, A.C., 1999. Nature and impact of the Neotectonic deformation in the western Sierra Nevada (Spain). Geomorphology 30, 259–272.

Sanz de Galdeano, C., Vera, J.A., 1992. Stratigraphic record and paleogeographical context of Neogene basins in the Betic Cordillera, Spain. Basin Research 4, 21–36.

Sanz de Galdeano, C., Rodríguez Fernández, J., López Garrido, A.C., 1991. Geologic map of the Alpujarran Corridor. Deposito Legal GR-830-1991, scale 1:50,000, 1 sheet.

Seidl, M.A., Dietrich, W.E., 1992. The problem of channel erosion into bedrock. Catena (Suppl. 23), 101–124.

Seidl, M.A., Dietrich, W.E., Kirchner, J.W., 1994. Longitudinal profile development into bedrock: an analyses of Hawaiian channels. Journal of Geology 102, 457–474.

Seidl, M.A., Finkel, R.C., Caffee, M.W., Bryant Hudson, G., Dietrich, W.E., 1997. Cosmogenic isotope analyses applied to river longitudinal profile evolution: problems and interpretations. Earth Surface Processes and Landforms 22, 195–209.

Sklar, L., Dietrich, W.E., 1998. River longitudinal profiles and bedrock incision models: stream power and the influence of sediment supply. In: Tinkler, K.J., Wohl, E.E. (Eds.), Rivers Over Rock: Fluvial Processes in Bedrock Channels. American Geophysical Union, Washington, DC, pp. 237–260.

Stock, J.D., Montgomery, D.R., 1999. Geologic constraints on bedrock river incision using the stream power law. Journal of Geophysical Research 104, 4983–4993.

Stokes, M., Mather, A.E., Harvey, A.M., 2002. Quantification of river-capture-induced base-level changes and landscape development, Sorbas Basin, SE Spain. In: Jones, S.J., Frostick, L.E. (Eds.), Sediment Fluxes to Basins: Causes, Controls, and Consequences. Geological Society of London Special Publications, vol. 191, pp. 23–35.

Tinkler, K.J., Wohl, E.E., 1998. A primer on bedrock channels. In: Tinkler, K.J., Wohl, E.E. (Eds.), Rivers Over Rock: Fluvial Processes in Bedrock Channels. American Geophysical Union, Washington, DC, pp. 1–18.

Tucker, K.J., Slingerland, R.L., 1994. Erosional dynamics, flexural isostasy, and long-lived escarpments: a numeric modeling study. Journal of Geophysical Research 99 (B6), 12229–12243.

Williams, D.F., Thunnel, R.C., Tappa, E., Río, D., Raffi, I., 1988. Chronology of the Pleistocene oxygen isotope record: 0–1.8 m.y.b.p. Paleogeography, Palaeoclimatology, Palaeoecology 64, 221–240.

Weissel, J.K., Seidl, M.A., 1998. Inland propagation of erosional escarpments and river profile evolution across the southeast Australian passive continental margin. In: Tinkler, K.J., Wohl, E.E. (Eds.), Rivers Over Rock: Fluvial Processes in Bedrock Channels. American Geophysical Union, Washington, DC, pp. 189–206.

Wohl, E.E., Merritt, D.M., 2001. Bedrock channel morphology. Geological Society of America Bulletin 113, 1205–1212.

Wright, V.P., Tucker, M.E., 1991. Calcretes: an introduction. In: Wright, V.P., Tucker, M.E. (Eds.), Calcretes. Blackwell, Oxford, pp. 1–22.

Zaprowski, B.J., Evenson, E.B., Pazzaglia, F.J., Epstein, J.B., 2001. Knickzone propagation in the Black Hills and northern High Plains: a different perspective on the late Cenozoic exhumation of the Laramide Rocky Mountains. Geology 29, 547–550.